

A DPF analysis yields accurate analytic potentials for $\text{Li}_2(a^3\Sigma_u^+)$ and $\text{Li}_2(1^3\Sigma_g^+)$ that incorporate 3-state mixing near the $1^3\Sigma_g^+$ -state asymptote

Nikesh S. Dattani,^a and Robert J. Le Roy^b

Department of Chemistry, University of Waterloo, Waterloo, ON N2L 3G1, Canada

(Dated: February 16, 2022)

A combined-isotopologue direct-potential-fit (DPF) analysis of optical and photoassociation spectroscopy data for the $a^3\Sigma_u^+$ and $1^3\Sigma_g^+$ states of Li_2 has yielded accurate analytic potential energy functions for both states. The recommended M3LR_{5,3}^{8,0}(3) potential for the $a^3\Sigma_u^+$ of $^7,^7\text{Li}_2$ has a well depth of $\mathfrak{D}_e = 333.758(7) \text{ cm}^{-1}$ and equilibrium distance of $r_e = 4.17005(3) \text{ \AA}$, and the associated scattering lengths are $a_{\text{SL}} = -14.759(9) \text{ \AA}$ for $^7,^7\text{Li}_2$ and $-1906(50) \text{ \AA}$ for $^6,^6\text{Li}_2$. For the $1^3\Sigma_g^+$ state, in spite of a gap of $\sim 5200 \text{ cm}^{-1}$ (from $v(1^3\Sigma_g^+) = 8 - 61$) for which there are no data, the DPF procedure has no difficulty determining an accurate overall potential. The $1^3\Sigma_g^+$ state of the $^7,^7\text{Li}_2$ isotopologue has a well depth of $\mathfrak{D}_e = 7092.417(33) \text{ cm}^{-1}$ and equilibrium distance of $r_e = 3.06524(9) \text{ \AA}$. The long-range tail of the recommended M3LR_{6,3}^{3,6}(9) potential energy function for the $1^3\Sigma_g^+$ state is defined by the lowest eigenvalue of a 3×3 long-range interstate coupling matrix to take into account the 3-state mixing near its asymptote.

^a Present address: Quantum Information Processing Building, Department of Materials, 12/13 Parks Road, OX1 3PH, UK: dattani.nike@gmail.com

^b leroy@uwaterloo.ca

I. INTRODUCTION

Modern theoretical studies of ultra-cold atomic gases demand a very accurate knowledge of the potential energy curves (PECs) of the systems of interest. Since Li_2 is the second smallest uncharged stable homonuclear molecule, its chemical and physical properties are particularly interesting. In recent years, considerable effort has been focussed on the lowest singlet states of Li_2 .^{1–10} However, the properties of the triplet states of Li_2 are much less well known.

The first observation of discrete spectra involving the lowest triplet state of Li_2 was reported in 1985 by Xie and Field,¹¹ who used perturbation-facilitated optical-optical double resonance (PFOODR) techniques to excite $2^3\Pi_g - a^3\Sigma_u^+$ emission. They observed transitions involving $v(a^3\Sigma_u^+) = 0 - 6$, but because of the limited resolution available at the time, their results have been superseded by later work. The first high-resolution triplet-system measurements were reported three years later by Martin *et al.*,¹² who performed a Fourier transform study of the $1^3\Sigma_g^+ \rightarrow a^3\Sigma_u^+$ system of $^7,^7\text{Li}_2$ involving $v' = 1 - 7$ of the upper state and $v'' = 0 - 7$ of the ground triplet state, with average measurement uncertainties of only $\pm 0.01 \text{ cm}^{-1}$. Analogous results for the same system of $^6,^6\text{Li}_2$, spanning the same ranges of vibrational levels, and with the same accuracy, were reported a year later by Linton *et al.*¹³ A decade later Linton *et al.*¹⁴ reported a high-resolution version of the PFOODR experiment of Xie and Field¹¹ which yielded accurate (uncertainties ranging from 0.005 to 0.001 cm^{-1}) observations of transitions into $v(a^3\Sigma_u^+) = 0 - 9$ from a handful of rotational levels of the $v' = 1$ and 2 levels of the $2^3\Pi_g$ state of $^7,^7\text{Li}_2$. In addition, a two-photon photoassociation spectroscopy (PAS) experiment by Abraham *et al.*¹⁵ had yielded a direct measurement of the $0.416(\pm 0.001) \text{ cm}^{-1}$ binding energy of the $v=10$, $N=0$ level of the $a^3\Sigma_u^+$ state of $^7,^7\text{Li}_2$.

In addition to the seven vibrational levels $v = 1 - 7$ of the $1^3\Sigma_g^+$ state observed in the emission experiments, the binding energies of levels $v = 62 - 90$ of $^7,^7\text{Li}_2$ and $v = 56 - 84$ of $^6,^6\text{Li}_2$ were measured in a PAS study by Abraham *et al.*¹⁶ However, to date there has been no reported attempt to bridge the 5100 cm^{-1} gap between the two sets of results in order to provide a global description of this state. This problem is illustrated by Fig. 1, which shows the regions of the $a^3\Sigma_u^+$ and $1^3\Sigma_g^+$ potentials associated with the currently available experimental data. The task of bridging the chasm for the $1^3\Sigma_g^+$ state is complicated by the fact that in the region very near the upper-state asymptote spanned by the PAS data, a transition from case (b) to case (c) coupling leads to a mixing of the $1^3\Sigma_g^+$ state with two other states that also have 1_g symmetry in this long-range ($r \gtrsim 20 \text{ \AA}$) region.

The only PECs which have been reported for the lowest triplet states ($a^3\Sigma_u^+$ and $1^3\Sigma_g^+$) of Li_2 , are point-wise, semiclassical RKR curves generated from Dunham or near-dissociation expansions for the vibrational energies and inertial rotation B_v constants.^{12–14} For the $1^3\Sigma_g^+$ upper state, those PECs were based only on data for vibrational levels $v' = 0 - 7$,^{12,13} since that work preceded the the photo-association spectroscopy (PAS) studies of this system.^{15,16} Thus, the best available potential for the $1^3\Sigma_g^+$ state provides no realistic predictions for those subsequently observed high vibrational levels, took no account of interactions with other states of Li_2 near the dissociation asymptote of $1^3\Sigma_g^+$, and did not incorporate the theoretically known inverse-power long-range behaviour. Finally, in all studies of these states to date, $^7,^7\text{Li}_2$ and $^6,^6\text{Li}_2$ were treated independently, and as a consequence, the effect of Born-Oppenheimer breakdown (BOB) in this system remains unknown.

The present work presents a fully quantum mechanical direct-potential-fit (DPF) data analysis which accounts for all of the optical and PAS data described above in terms of global analytic potential energy functions for the $a^3\Sigma_u^+$ and $1^3\Sigma_g^+$ states of Li_2 , while independent term values are used to represent the 20 levels of the $2^3\Pi_g$ state giving rise to the observed high-resolution emission into $v(a^3\Sigma_u^+) = 0 - 9$. The three longest-range inverse-power contributions to the interaction energy are incorporated into the $a^3\Sigma_u^+$ and $1^3\Sigma_g^+$ state potential energy functions, and the function for the $1^3\Sigma_g^+$ state explicitly accounts for the three-state mixing referred to above. In addition, the incorporation of adiabatic Born-Oppenheimer breakdown (BOB) correction functions in the Hamiltonians for the $a^3\Sigma_u^+$ and $1^3\Sigma_g^+$ states allows the data for the two isotopologues to be treated simultaneously.

Three aspects of this system made its analysis unusually challenging. Firstly, the long-range tail of the $1^3\Sigma_g^+$ state PEC is not the familiar sum of simple inverse-power terms, since the $1^3\Sigma_g^+$ state couples strongly to two other states near the dissociation asymptote (see § II.C.1). Secondly, the fact that the leading long-range term of the PEC tail for the $1^3\Sigma_g^+$ state is C_3/r^3 means that the Morse/long-range (MLR) potential function leads to unphysical long-range behavior if not addressed appropriately (see § II.C.3).¹⁰ Finally, as illustrated by Fig. 1, the data for the $1^3\Sigma_g^+$ state has gaps from $v = 7$ to $v = 62$ for $^7,^7\text{Li}_2$ and from $v = 7$ to $v = 56$ for $^6,^6\text{Li}_2$, which span more than 72% of the well depth. Such a large gap in experimental information has never (to our knowledge) been treated successfully by a potential-fit analysis in a purely empirical manner.

II. MODELS AND METHODOLOGY

A. DPF Data Analyses and the Radial Hamiltonian

In a DPF spectroscopic data analysis, the upper and lower level of every observed energy transition is assumed to be an eigenvalue of an effective radial Schrödinger equation characterized by a parameterized potential energy function and (when appropriate) parameterized radial strength functions characterizing appropriate BOB terms. Given some plausible initial trial parameter values for characterizing the relevant potential, solution of the associated Schrödinger equation yields an eigenvalue $E_{v,J}$ and eigenfunction $\psi_{v,J}(r)$ for each observed level. The difference between the energies of appropriate upper and lower levels then yields an estimate of each observed transition energy, while use of the Hellmann-Feynman theorem:

$$\frac{\partial E_{v,J}}{\partial p_j} = \left\langle \psi_{v,J}(r) \left| \frac{\partial \hat{H}}{\partial p_j} \right| \psi_{v,J}(r) \right\rangle, \quad (1)$$

yields the partial derivatives required for performing a least-squares fit of the simulated transitions to the experimental data.

Since the observed transition energies are not linear functions of the parameters defining the effective radial Hamiltonian, a DPF analysis requires the use of an iterative non-linear least-squares fitting procedure. The quality of a given fit is characterized by the value of the dimensionless root-mean-square deviation of the N experimental data $y_{\text{obs}}(i)$ from the predicted values $y_{\text{calc}}(i)$

generated from the relevant Hamiltonian(s):

$$\overline{dd} \equiv \sqrt{\frac{1}{N} \sum_{i=1}^N \left(\frac{y_{\text{calc}}(i) - y_{\text{obs}}(i)}{u(i)} \right)^2}, \quad (2)$$

in which $u(i)$ is the uncertainty in the reported value of experimental datum i . In the present work, these fits were performed using the publicly available program **DPOTFIT**,¹⁷ while the requisite initial estimates of the potential function parameters were obtained using the program **betaFIT**¹⁸ with preliminary RKR potentials generated using conventional Dunham expansions.

As with most diatomic DPF analyses reported to date, the present work is based on the effective radial Schrödinger equation presented by Watson,^{19,20} and uses the conventions described in Refs. 21 and 22. In particular, the rovibrational levels of isotopologue α of diatomic molecule AB in a given electronic state are the eigenvalues of the radial Schrödinger equation:

$$\left\{ -\frac{\hbar^2}{2\mu_\alpha} \frac{d^2}{dr^2} + \left[V_{\text{ad}}^{(1)}(r) + \Delta V_{\text{ad}}^{(\alpha)}(r) \right] + \frac{\hbar^2 J(J+1)}{2\mu_\alpha r^2} [1 + g^{(\alpha)}(r)] \right\} \psi_{v,J}(r) = E_{v,J} \psi_{v,J}(r), \quad (3)$$

in which $V_{\text{ad}}^{(1)}(r)$ is the effective adiabatic internuclear potential for a selected reference isotopologue labeled $\alpha=1$, $\Delta V_{\text{ad}}^{(\alpha)}(r) = V_{\text{ad}}^{(\alpha)}(r) - V_{\text{ad}}^{(1)}(r)$ is the *difference* between the effective adiabatic potentials for isotopologue- α and isotopologue-1, $g^{(\alpha)}(r)$ is the non-adiabatic centrifugal-potential correction function for isotopologue- α , and the reduced mass μ_α is defined by the atomic masses $M_{\text{A}}^{(\alpha)}$ and $M_{\text{B}}^{(\alpha)}$. Following standard conventions,^{19–23} the BOB terms $\Delta V_{\text{ad}}^{(\alpha)}(r)$ and $g^{(\alpha)}(r)$ are both written as a sum of contributions from component atoms A and B:

$$\Delta V_{\text{ad}}^{(\alpha)}(r) = \frac{\Delta M_{\text{A}}^{(\alpha)}}{M_{\text{A}}^{(\alpha)}} \tilde{S}_{\text{ad}}^{\text{A}}(r) + \frac{\Delta M_{\text{B}}^{(\alpha)}}{M_{\text{B}}^{(\alpha)}} \tilde{S}_{\text{ad}}^{\text{B}}(r), \quad (4)$$

$$g^{(\alpha)}(r) = \frac{M_{\text{A}}^{(1)}}{M_{\text{A}}^{(\alpha)}} \tilde{R}_{\text{na}}^{\text{A}}(r) + \frac{M_{\text{B}}^{(1)}}{M_{\text{B}}^{(\alpha)}} \tilde{R}_{\text{na}}^{\text{B}}(r), \quad (5)$$

in which $\Delta M_{\text{A/B}}^{(\alpha)} = M_{\text{A/B}}^{(\alpha)} - M_{\text{A/B}}^{(1)}$ are the differences between the atomic masses of atoms A or B in isotopologue- α and in isotopologue-1. In the present case $\text{A}=\text{B}=\text{Li}$, and these expressions collapse to

$$\Delta V_{\text{ad}}^{(\alpha)}(r) = \left(\frac{\Delta M_{\text{Li}^a}^{(\alpha)}}{M_{\text{Li}^a}^{(\alpha)}} + \frac{\Delta M_{\text{Li}^b}^{(\alpha)}}{M_{\text{Li}^b}^{(\alpha)}} \right) \tilde{S}_{\text{ad}}^{\text{Li}}(r) \quad (6)$$

$$g^{(\alpha)}(r) = \left(\frac{M_{\text{Li}^a}^{(1)}}{M_{\text{Li}^a}^{(\alpha)}} + \frac{M_{\text{Li}^b}^{(1)}}{M_{\text{Li}^b}^{(\alpha)}} \right) \tilde{R}_{\text{na}}^{\text{Li}}(r). \quad (7)$$

Although only a single radial strength function of each type must be considered in the present case ($\tilde{S}_{\text{ad}}^{\text{Li}}(r)$ and $\tilde{R}_{\text{na}}^{\text{Li}}(r)$), two mass factors must be retained in order to allow us to describe all possible molecular isotopologues.

B. The ‘Basic’ Morse/Long-Range (MLR) Potential Energy Function

The next step is to introduce an optimal analytic function for representing the effective adiabatic internuclear potential for the reference isotopologue, $V_{\text{ad}}^{(1)}(r) \equiv V(r)$. The present work is based on use of the version of the Morse/long-range (MLR) potential energy function of Refs. 10 and 24,

$$V_{\text{MLR}}(r) = \mathfrak{D}_e \left[1 - \frac{u_{\text{LR}}(r)}{u_{\text{LR}}(r_e)} e^{-\beta(r) \cdot y_p^{\text{eq}}(r)} \right]^2, \quad (8)$$

in which \mathfrak{D}_e is the well depth, r_e the equilibrium internuclear distance, and the radial variable in the exponent is

$$y_p^{\text{eq}}(r) \equiv \frac{r^p - r_e^p}{r^p + r_e^p}. \quad (9)$$

The parameterized exponent coefficient function $\beta(r)$ which governs the details of the shape of the potential is defined so that

$$\lim_{r \rightarrow \infty} \beta(r) \equiv \beta_\infty = \ln \left(\frac{2\mathfrak{D}_e}{u_{\text{LR}}(r_e)} \right), \quad (10)$$

and as a result, the long-range behavior of the potential energy function is defined by the function $u_{\text{LR}}(r)$:

$$V_{\text{MLR}}(r) \simeq \mathfrak{D}_e - u_{\text{LR}}(r) + \mathcal{O}(u_{\text{LR}}(r)^2/4\mathfrak{D}_e), \dots, \quad (11)$$

while the denominator factor $u_{\text{LR}}(r_e)$ is simply the value of that long-range tail function evaluated at the equilibrium bond length.

The theory of long-range intermolecular forces shows us that in general, $u_{\text{LR}}(r)$ may be written in the form

$$u_{\text{LR}}(r) = \sum_{i=1}^{\text{last}} D_m(r) \frac{C_{m_i}}{r^{m_i}}. \quad (12)$$

in which the powers m_i and coefficients C_{m_i} of the terms contributing to this sum are determined by the symmetry of the given electronic state and the nature of the atoms to which it dissociates,^{25–28} and the ‘damping functions’ $D_m(r)$ were introduced to take account of the weakening of the interaction energies associated with these simple inverse-power terms due to overlap of the electronic wavefunctions on the interacting atoms.²⁹ While most previous applications of the MLR potential function form omitted the $D_m(r)$ damping function factors, it was shown in Ref. 24 that in addition to providing a more realistic physical description of the long-range potential tail, their introduction improves the extrapolation behaviour of the repulsive short-range potential wall, and when they are included, fewer parameters are required to achieve a given quality of fit to experimental data. In either case, the structure of Eq.(11) means that at large distances where $u_{\text{LR}}(r) \gg u_{\text{LR}}(r)^2/(4\mathfrak{D}_e)$, the long-range behaviour of V_{MLR} is defined by $u_{\text{LR}}(r)$.

Following Ref. 24, the present work uses the modified Douketis-type³⁰ damping function form

$$D_m^{\text{DS}(s)}(r) = \left(1 - e^{-\frac{b^{\text{ds}}(s)(\rho r)}{m} - \frac{c^{\text{ds}}(s) \cdot (\rho r)^2}{\sqrt{m}}} \right)^{m+1}, \quad (13)$$

with $s = -1$. Here, $b^{\text{ds}}(s)$ and $c^{\text{ds}}(s)$ are treated as system-independent parameters with $b^{\text{ds}}(-1) = 3.30$ and $c^{\text{ds}}(-1) = 0.423$. For interacting atoms A and B, $\rho \equiv \rho_{\text{AB}} = 2\rho_{\text{A}}\rho_{\text{B}}/(\rho_{\text{A}} + \rho_{\text{B}})$, in which

$\rho_A = (I_p^A/I_p^H)^{2/3}$ is defined in terms the ionization potential of the atom A and that of an H atom (I_p^A and I_p^H respectively). Inclusion of these damping functions means that at very short distances $V_{\text{MLR}}(r) \propto 1/r^2$.²⁴ Comparisons with *ab initio* results for a sampling of chemical and Van der Waals interactions showed that this type of damping function yielded quite realistic MLR short-range extrapolation behaviour,²⁴ so this $D_m(r)$ form is adopted here.

In order to ensure that the exponent coefficient function in Eq. (8) satisfies Eq. (10), it is customary to write it as the constrained polynomial:

$$\beta(r) = \beta_p^q(r) \equiv y_p^{\text{ref}}(r) \beta_\infty + [1 - y_p^{\text{ref}}(r)] \sum_{i=0}^N \beta_i [y_q^{\text{ref}}(r)]^i. \quad (14)$$

This function is expressed in terms of two radial variables which are similar to $y_p^{\text{eq}}(r)$, but are defined with respect to a different expansion center (r_{ref}), and involve two different powers, p and q (the reasons for this structure are discussed in Ref. 10):

$$y_p^{\text{ref}}(r) \equiv \frac{r^p - r_{\text{ref}}^p}{r^p + r_{\text{ref}}^p} \quad \text{and} \quad y_q^{\text{ref}}(r) \equiv \frac{r^q - r_{\text{ref}}^q}{r^q + r_{\text{ref}}^q}. \quad (15)$$

The limiting long-range behaviour of the exponential term in Eq. (8) gives rise to additional inverse-power contributions to the long-range potential of Eq. (11), with the leading term being proportional to $1/r^{m_1+p}$. This means that the power p must be greater than $(m_{\text{last}} - m_1)$ if the long-range behaviour of Eq. (12) is to be maintained.¹⁰ There is no analogous formal constraint on the value of q ; however, experience suggests that its value should lie in the range $2 \lesssim q \leq p$.^{10,24,32} In early work with this potential function form, the radial variables in Eq. (14) were both defined as $y_p^{\text{eq}}(r)$ of Eq. (9) (i.e., $r_{\text{ref}} = r_e$ and $q = p$).^{31,33-35} However, it has since been shown that setting $r_{\text{ref}} > r_e$ and $q < p$ can significantly reduce the number of β_i parameters required to describe a given data set accurately, and yields more stable expansions.^{10,24,32}

A second consideration associated with the use of the damping functions of Eq. (13) is their effect on the shape of the short-range repulsive potential wall of an MLR potential. As was pointed out in Ref. 24, the fact that the radial variables $y_{p/q}^{\text{ref}}(r) \rightarrow -1$ as $r \rightarrow 0$ means that at very small distances $V_{\text{MLR}}(r) \propto \{u_{\text{LR}}(r)\}^2$. If damping functions are neglected (i.e., if Eq. (12) did not include the $D_m(r)$ functions), then the limiting short-range behaviour of the potential energy function would be $V_{\text{MLR}}(r) \propto 1/r^{2m_{\text{last}}}$. However, for a typical two- or three-term $u_{\text{LR}}(r)$ expansion, $m_{\text{last}} = 8$ or 10, and the resulting $1/r^{16}$ or $1/r^{20}$ short-range repulsive wall behaviour would be unphysically excessively steep. In the data-sensitive region of the potential well, this excessive growth rate would be compensated for by the behaviour of the empirically determined exponent coefficient function $\beta(r)$. However, the unphysical high-order r^{-16} or r^{-20} singular behaviour would re-assert itself in the shorter-range extrapolation region.

In this paper, the label for particular MLR potential function models is written as $\text{MxLR}_{p,q}^{r_{\text{ref}}}(N)$, in which x is the number of inverse-power terms incorporated into $u_{\text{LR}}(r)$, while p , q , r_{ref} and N are defined above. The ‘basic’ MLR model described above is used herein to describe the potential energy function for the $a^3\Sigma_u^+$ state of Li_2 . However, some enhancements were required for treating the $1^3\Sigma_g^+$ state.

C. Modified MLR Potential for the $1^3\Sigma_g^+$ State of Li_2

1. Incorporating interstate coupling into the MLR model

At a preliminary stage of the present work, the $1^3\Sigma_g^+$ state of Li_2 was represented by the ‘basic’ MLR function of Eqs. (8)–(15), in which $u_{\text{LR}}(r)$ consisted of three terms, with $m_i = \{3, 6, 8\}$. Because of the added complexity due to interstate coupling near the dissociation asymptote, all damping functions for this state were fixed at $D_m(r) = 1$. This model was able to provide an excellent fit both to the fluorescence data for $v' = 0 - 7$, and to the $^{7,7}\text{Li}_2$ PAS data for $v = 62 - 70$ and the $^{6,6}\text{Li}_2$ PAS data for $v = 56 - 65$ whose upper limits which correspond to binding energies of about 24 cm^{-1} . However, when PAS data for higher vibrational levels were included in the analysis, the quality of fit got progressively worse, and the discrepancies could not easily be removed simply by increasing the order of the polynomial $\beta(r)$. The reason for this increasing inability of the basic MLR model to account for levels lying very near dissociation is that the $1^3\Sigma_g^+$ state of Li_2 couples to two other states near its dissociation asymptote.

This same type of problem was encountered in a recent study of the $A(^1\Sigma_u^+) - X(^1\Sigma_g^+)$ system of Li_2 . In that case the $0_u^+(A^1\Sigma_u^+)$ state which goes to the $\text{Li}(^2P_{1/2}) + \text{Li}(^2S_{1/2})$ asymptote couples to the $0_u^+(b^3\Pi)$ state which goes to the higher $\text{Li}(^2P_{3/2}) + \text{Li}(^2S_{1/2})$ limit,^{36,37} and the energies of levels lying near dissociation could not be explained properly without taking account of the inter-state mixing. Fortunately, Aubert-Frécon and co-workers had derived an analytic description of those coupled states based on the eigenvalues of a 2×2 interaction matrix,^{5,37} and it was shown that their analytic expression for the lower eigenvalue could readily be used to define $u_{\text{LR}}(r)$ for this state in an MLR potential model.¹⁰

Treatment of levels lying near the dissociation limit of the $1^3\Sigma_g^+$ state of Li_2 involves a similar problem; while it dissociates to the $\text{Li}(^2P_{1/2}) + \text{Li}(^2S_{1/2})$ limit, it couples to $1_g(^1\Pi)$ and $1_g(^3\Pi)$ states which correlate with the higher $\text{Li}(^2P_{3/2}) + \text{Li}(^2S_{1/2})$ limit.^{36,37} Since the $\text{Li}(^2P)$ state spin-orbit splitting is quite small (ca. 0.335 cm^{-1}), the interstate coupling only becomes important for levels lying relatively close to the dissociation limit. Fortunately, Aubert-Frécon and co-workers have studied this case too.³⁷ In particular, they presented expressions for the six independent elements of the symmetric 3×3 matrix that defines the long-range interaction energies for these three states. Their matrix elements took into account the first-order resonance-dipole ($1/r^3$) term, the leading dispersion energy terms, and the exchange energy. If we neglect the exchange term, keep only the first two ($m = 6$ and 8) dispersion energy terms, set the zero of energy at the $1^3\Sigma_g^+$ -state asymptote, make use of the symmetry relation for $m = 3$,

$$C_3^{3\Sigma_g^+} = 2C_3^{1\Pi_g} = -2C_3^{3\Pi_g} \equiv C_3^\Sigma, \quad (16)$$

and that for $m = 6$,

$$C_6^{1\Pi_g} = C_6^{3\Pi_g} \equiv C_6^\Pi, \quad (17)$$

and define $C_{6,8}^\Sigma \equiv C_{6,8}^{3\Sigma_g^+}$, their 3×3 long-range interaction matrix \mathbf{M}_{LR} becomes

$$\begin{pmatrix} -\frac{1}{3} \left(\frac{C_3^\Sigma}{r^3} + \frac{C_6^\Sigma + 2C_6^\Pi}{r^6} + \frac{C_8^\Sigma + C_8^{1\Pi_g} + C_8^{3\Pi_g}}{r^8} \right) & \frac{\sqrt{2}}{3} \left(\frac{C_3^\Sigma}{r^3} + \frac{C_6^\Sigma - C_6^\Pi}{r^6} + \frac{2C_8^\Sigma - C_8^{1\Pi_g} - C_8^{3\Pi_g}}{2r^8} \right) & \frac{1}{\sqrt{6}} \left(\frac{C_3^\Sigma}{r^3} + \frac{C_8^{1\Pi_g} - C_8^{3\Pi_g}}{r^8} \right) \\ \frac{\sqrt{2}}{3} \left(\frac{C_3^\Sigma}{r^3} + \frac{C_6^\Sigma - C_6^\Pi}{r^6} + \frac{2C_8^\Sigma - C_8^{1\Pi_g} - C_8^{3\Pi_g}}{2r^8} \right) & -\frac{2}{3} \left(\frac{C_3^\Sigma}{r^3} + \frac{2C_6^\Sigma + C_6^\Pi}{2r^6} + \frac{4C_8^\Sigma + C_8^{1\Pi_g} + C_8^{3\Pi_g}}{4r^8} \right) + \Delta E & \frac{1}{2\sqrt{3}} \left(\frac{C_3^\Sigma}{r^3} + \frac{C_8^{1\Pi_g} - C_8^{3\Pi_g}}{r^8} \right) \\ \frac{1}{\sqrt{6}} \left(\frac{C_3^\Sigma}{r^3} + \frac{C_8^{1\Pi_g} - C_8^{3\Pi_g}}{r^8} \right) & \frac{1}{2\sqrt{3}} \left(\frac{C_3^\Sigma}{r^3} + \frac{C_8^{1\Pi_g} - C_8^{3\Pi_g}}{r^8} \right) & - \left(\frac{C_6^\Pi}{r^6} + \frac{C_8^{1\Pi_g} + C_8^{3\Pi_g}}{2r^8} \right) + \Delta E \end{pmatrix}, \quad (18)$$

in which ΔE is the accurately known (positive) spin-orbit splitting energy of $\text{Li}(^2P)$.³⁸ Note that in contrast with Ref. 37, the present formulation treats attractive C_m coefficients as positive, rather than negative quantities. Following the correlation scheme given by Movre and Pichler,³⁶ the lowest eigenvalue of the matrix (18) defines the long-range tail of the $1^3\Sigma_g^+$ -state interaction potential; see Fig. 2.

Analytic expressions for the three eigenvalues of Eq. (18) were reported in Ref. 37. Those expressions for the zeros of the characteristic polynomial for \mathbf{M}_{LR} were obtained using the method of Scipione del Ferro and Niccolò Fontana Tartaglia (first published³⁹ by Gerolamo Cardano in 1545), and by applying a trigonometric substitution to avoid expressions involving square-roots of negative quantities. However, Kopp has demonstrated that while it is useful for obtaining symbolic expressions, this formula can yield substantial errors when used for actual computations, primarily because of the numerical errors that accumulate when computing the arctan function within the formula.⁴⁰ Moreover, the symbolic expressions for the derivatives of the lowest eigenvalue with respect to the $C_n^{\Sigma/\Pi}$ coefficients required by the least-squares fitting procedure are inconveniently complex. Because of these problems, in the present work the eigenvalues of this interaction matrix were calculated numerically (using the Jacobi eigenvalue algorithm^{40,41}), and their derivatives with respect to the $C_n^{\Sigma/\Pi}$ coefficients were computed using the discrete version of the Hellmann-Feynman theorem:

$$\frac{d\lambda_i}{dp} = \left\langle \phi_\lambda \left| \frac{d\mathbf{M}_{\text{LR}}}{dp} \right| \phi_\lambda \right\rangle, \quad (19)$$

in which λ_i is the appropriate eigenvalue of the matrix \mathbf{M}_{LR} , and ϕ_{λ_i} is the corresponding eigenvector.

2. Simplifying the treatment of interstate coupling for $\text{Li}_2(1^3\Sigma_g^+)$

The treatment of the long-range behaviour of the $A^1\Sigma_u^+$ state of Li_2 in Ref. 10 was precisely analogous to that for the $1^3\Sigma_g^+$ state discussed here, except that while that case involved a 2×2 matrix whose eigenvalues were determined analytically, the present case involves the 3×3 matrix of Eq. (18) whose eigenvalues are calculated numerically. In the treatment of the $A^1\Sigma_u^+$ state, it was shown that the C_6^Π/r^6 and C_8^Π/r^8 terms had virtually no effect on the lower (Σ -state) eigenvalue of the 2×2 long-range interstate coupling matrix. This led us to consider making the same simplification here.

Following the approach of Ref. (10), we compared the values of the lowest eigenvalue of Eq. (18) obtained when all $C_6^{\Sigma/\Pi}$ and $C_8^{\Sigma/\Pi}$ coefficients were defined by the theoretical values of Tang *et al.*,⁴² with those obtained on setting $C_6^\Pi = C_8^\Pi = C_8^{3\Pi_g} = 0$. Over the range $r = 2$ to 500 \AA , the

difference between these two estimates of the lowest eigenvalue were always less than $3 \times 10^{-6} \text{ cm}^{-1}$. Thus, it seems clear that in the present treatment of the $1^3\Sigma_g^+$ state of Li_2 , no significant errors will be introduced if contributions involving C_6^Π , $C_8^{1\Pi_g}$ and $C_8^{3\Pi_g}$ are omitted from Eq. (18). At the same time, it is important to note that these C_6^Π and C_8^Π coefficients *cannot* be neglected when using the two higher eigenvalues of Eq. (18) to define the long-range tails of the $3\Pi_g$ and $1\Pi_g$ states which couple with the $1^3\Sigma_g^+$ state of interest here. This point is illustrated by Fig. 3, which compares plots of the three eigenvalues of Eq. (18) obtained using all of the $C_n^{\Sigma/\Pi}$ coefficients of Tang *et al.*⁴² (solid red curves) with those obtained from this same matrix when $C_6^\Pi = 0 = C_8^{1\Pi_g} = C_8^{3\Pi_g}$ (dashed blue curves). It is clear that at the smaller distances where the C_6 and C_8 terms become important, one cannot use the above approximation when calculating the eigenvalues of (18) associated with the two Π_g states.

3. Implications of the quadratic term in the MLR potential function form

It was shown in Ref. 10 that contributions from the quadratic term in Eq. (11) can give rise to spurious perturbations in long-range behavior of the MLR potential function form. In the present case, the leading terms in the long-range potential for the $1^3\Sigma_g^+$ state of Li_2 correspond to $m_i = \{3, 6, 8\}$. If we temporarily ignore the effects of damping and interstate coupling in order to write $u_{\text{LR}}(r)$ as a simple inverse-power sum, the presence of the quadratic term in Eqs. (8) and (11) mean that the effective long-range behavior of the MLR potential would be

$$V_{\text{MLR}}(r) \simeq \mathfrak{D}_e - \frac{C_3}{r^3} - \frac{C_6}{r^6} - \frac{C_8}{r^8} + \frac{(C_3)^2/(4\mathfrak{D}_e)}{r^6} + \frac{C_3 C_6/(2\mathfrak{D}_e)}{r^9} + \dots \quad (20)$$

Thus, if the overall effective long-range behavior is to be defined by an inverse-power sum governed by the specified C_3 , C_6 and C_8 coefficients (and *not* include the last two terms in Eq. (20)!), the definition of $u_{\text{LR}}(r)$ must compensate for the quadratic terms by being defined as

$$u_{\text{LR}}(r) = \frac{C_3}{r^3} + \frac{C_6^{\text{adj}}}{r^6} + \frac{C_8}{r^8} + \frac{C_9^{\text{adj}}}{r^9}, \quad (21)$$

in which $C_6^{\text{adj}} \equiv C_6 + (C_3)^2/(4\mathfrak{D}_e)$ and $C_9^{\text{adj}} \equiv C_3 C_6^{\text{adj}}/(2\mathfrak{D}_e)$.

Since the long-range tail of our $1^3\Sigma_g^+$ -state potential also includes interstate coupling, these expressions for C_6^{adj} and C_9^{adj} (which were derived analytically for potentials with simpler long-range tails) need to be tested in order to determine how well they cancel the effect of the spurious last-two terms in Eq. (20). Results of a numerical test of this question are presented in Fig. 4, which displays plots of the quantity $C_3^{\text{eff}}(r) \equiv r^3[\mathfrak{D} - u_{\text{LR}}(r)]$ *vs.* r^{-3} for three different definitions of $u_{\text{LR}}(r)$. This type of plot illustrates the nature of the long-range interaction on a reduced scale. If $u_{\text{LR}}(r)$ was defined as the simple inverse-power sum of Eq. (21), as $r^{-3} \rightarrow 0$ the resulting plot would approach an intercept of C_3 with a limiting slope of C_6^{eff} . In the present case, however, the three-state coupling near the potential asymptote causes all of the plots in Fig. 4 to drop off sharply for $r^{-3} \lesssim 10^{-4} \text{ \AA}^{-3}$.

The desired long-range behavior is achieved when $u_{\text{LR}}(r)$ is defined simply as the lowest eigenvalues of the matrix of Eq. (18), $u_{\text{LR}}(r) = -\lambda_{\text{min}}(r)$. For the case in which $C_6^\Pi = C_8^{1\Pi_g} = C_8^{3\Pi_g} = 0$ and the other $C_n^{\Sigma/\Pi}$ coefficients are fixed at the values of Tang *et al.*,⁴² this desired behavior is

defined by the solid black curve in Fig. 4. The dash-dot-dot red curve in Fig. 4 then shows how the long-range behavior of the associated MLR potential, which includes the quadratic term of Eq. (11), deviates from this desired long-range behavior. Next, the dotted blue curve shows the effect on the long-range MLR behavior of replacing C_6^Σ by the quantity C_6^{adj} defined above. It is immediately clear that this removes most of the discrepancy with the ‘ideal’ long-range behavior (solid black curve). Finally, the dashed green curve shows the effect on the long-range MLR potential tail of also including the C_9^{adj}/r^9 term in the definition of $u_{\text{LR}}(r)$ in order to cancel out the spurious r^{-9} term in Eq. (21). It is clear that use of the resulting definition

$$u_{\text{LR}}(r) = -\lambda_{\min}(C_3, C_6^{\text{adj}}, C_8; r) + C_9^{\text{adj}}/r^9 \quad (22)$$

brings the long-range tail of the overall MLR potential function into essentially exact agreement with the desired form.

4. Inclusion of retardation in the model potential for $\text{Li}_2(1^3\Sigma_g^+)$

It has long been known that at the very large distances where the C_3/r^3 term comes to dominate the interaction energy in this type of system, “retardation” effects due to the finite speed of light should not be neglected.^{43,44} It was shown by Meath⁴⁴ that the effect of retardation on an s/p resonance-dipole interaction can be accounted for by multiplying C_3^Σ by the function $f_{\text{ret}}^\Sigma(r)$ and C_3^Π by the function $f_{\text{ret}}^\Pi(r)$, where

$$f_{\text{ret}}^\Sigma = \cos\left(\frac{r}{\lambda_{SP}}\right) + \left(\frac{r}{\lambda_{SP}}\right) \sin\left(\frac{r}{\lambda_{SP}}\right) \quad (23)$$

$$f_{\text{ret}}^\Pi = f_{\text{ret}}^\Sigma - \left(\frac{r}{\lambda_{SP}}\right)^2 \cos\left(\frac{r}{\lambda_{SP}}\right), \quad (24)$$

in which $\lambda_{SP} = \lambda_{SP}/2\pi$ and λ_{SP} is the wavelength of light associated with the atomic $^2S - ^2P$ transition.

It is a straightforward matter to incorporate this retardation behavior into the MLR potential function form. In particular, on setting $C_6^\Pi = C_8^\Pi = 0$, making use of the symmetry relationships among the C_3^Σ , $C_3^{\Pi_g}$ and $C_3^{\Pi_g}$ coefficients, and replacing C_6^Σ by $C_6^{\Sigma, \text{adj}}$, the long-range interstate coupling matrix for the three 1_g states dissociating to yield $\text{Li}(^2S_{1/2}) + \text{Li}(^2P)$ becomes

$$\mathbf{M}_{\text{LR}} = \begin{pmatrix} -\frac{1}{3} \left(\frac{C_3^\Sigma f_{\text{ret}}^\Sigma}{r^3} + \frac{C_6^{\Sigma, \text{adj}}}{r^6} + \frac{C_8^\Sigma}{r^8} \right) & \frac{\sqrt{2}}{3} \left(\frac{C_3^\Sigma f_{\text{ret}}^\Sigma}{r^3} + \frac{C_6^{\Sigma, \text{adj}}}{r^6} + \frac{C_8^\Sigma}{r^8} \right) & \frac{1}{\sqrt{6}} \frac{C_3^\Sigma f_{\text{ret}}^\Pi}{r^3} \\ \frac{\sqrt{2}}{3} \left(\frac{C_3^\Sigma f_{\text{ret}}^\Sigma}{r^3} + \frac{C_6^{\Sigma, \text{adj}}}{r^6} + \frac{C_8^\Sigma}{r^8} \right) & -\frac{2}{3} \left(\frac{C_3^\Sigma f_{\text{ret}}^\Sigma}{r^3} + \frac{C_6^{\Sigma, \text{adj}}}{r^6} + \frac{C_8^\Sigma}{r^8} \right) + \Delta E & \frac{1}{2\sqrt{3}} \frac{C_3^\Sigma f_{\text{ret}}^\Pi}{r^3} \\ \frac{1}{\sqrt{6}} \frac{C_3^\Sigma f_{\text{ret}}^\Pi}{r^3} & \frac{1}{2\sqrt{3}} \frac{C_3^\Sigma f_{\text{ret}}^\Pi}{r^3} & \Delta E \end{pmatrix}. \quad (25)$$

Unless stated otherwise, the definition of the long-range tail of the MLR potential for the $1^3\Sigma_g^+$ used throughout the rest of this study is therefore given by

$$u_{\text{LR}}^{\text{ret}}(r) = -\lambda_{\min}^{\text{ret}}(C_3^\Sigma, C_6^{\text{adj}}, C_8^\Sigma; r) + C_9^{\text{adj}}/r^9 \quad (26)$$

in which $\lambda_{\min}^{\text{ret}}(C_3^\Sigma, C_6^{\text{adj}}, C_8^\Sigma; r)$ is the lowest eigenvalue of the interaction energy matrix of Eq. (25).

D. Born-Oppenheimer Breakdown Functions

The radial strength functions in Eqs. (6) and (7) may be written as polynomials constrained to have specified asymptotic values using the format of Eq. (14)

$$\tilde{S}_{\text{ad}}^{\text{Li}}(r) = y_{p_{\text{ad}}}^{\text{eq}}(r) u_{\infty}^{\text{Li}} + [1 - y_{p_{\text{ad}}}^{\text{eq}}(r)] \sum_{i=0} u_i^{\text{Li}} y_{q_{\text{ad}}}^{\text{eq}}(r)^i \quad (27)$$

$$\tilde{R}_{\text{na}}^{\text{Li}}(r) = y_{p_{\text{na}}}^{\text{eq}}(r) t_{\infty}^{\text{Li}} + [1 - y_{p_{\text{na}}}^{\text{eq}}(r)] \sum_{i=0} t_i^{\text{Li}} y_{q_{\text{na}}}^{\text{eq}}(r)^i \quad (28)$$

in which u_{∞}^{Li} and t_{∞}^{Li} are the values of these functions in the limit $r \rightarrow \infty$, u_0^{Li} and t_0^{Li} define their values at $r = r_e$, and the radial variables are versions of Eq. (9) associated with chosen values of the integers p_{ad} , p_{na} , q_{ad} and q_{na} .²² The discussion of Ref. 22 shows that $t_{\infty}^{\text{A}} = 0.0$ for any molecule which dissociates to yield an uncharged atom-A, so $t_{\infty}^{\text{Li}}(a^3\Sigma_u^+) = t_{\infty}^{\text{Li}}(1^3\Sigma_g^+) = 0.0$. In addition, we adopt the Watson convention of setting the parameter $t_0^{\text{Li}} = 0.0$ for both the $a^3\Sigma_u^+$ and $1^3\Sigma_g^+$ states, since its value cannot be determined from transition-frequency data alone.^{19,20,22}

Following standard conventions,²¹ the absolute zero of energy is defined as the energy of ground-state atoms separated at $r \rightarrow \infty$, so by definition $u_{\infty}^{\text{Li}}(a^3\Sigma_u^+) = 0.0$. Since the $1^3\Sigma_g^+$ state of Li_2 dissociates to one ground-state ($^2S_{1/2}$) and one excited-state ($^2P_{1/2}$) atom, the value of $u_{\infty}^{\text{Li}}(1^3\Sigma_g^+)$ is then defined by the difference between the atomic $^2P_{1/2} \leftarrow ^2S_{1/2}$ excitation energies for ^6Li and ^7Li , which is^{21,38}

$$\delta E_{7\text{Li}}^{6\text{Li}}(^2P_{1/2}) = \Delta E^{6\text{Li}}(^2P_{1/2} \leftarrow ^2S_{1/2}) - \Delta E^{7\text{Li}}(^2P_{1/2} \leftarrow ^2S_{1/2}) = -0.351\,338 \text{ [cm}^{-1}] \quad (29)$$

This is the difference between the energy asymptotes of the $1^3\Sigma_g^+$ states of $^6,^6\text{Li}_2$ and $^7,^7\text{Li}_2$, and it defines the asymptotic value of the adiabatic radial strength function.²¹ Since we select $^7,^7\text{Li}_2$ as the reference isotopologue, this yields

$$u_{\infty}^{\text{Li}}(1^3\Sigma_g^+) = \delta E_{7\text{Li}}^{6\text{Li}}(^2P_{1/2}) / 2 \left(1 - \frac{M(^7\text{Li})}{M(^6\text{Li})} \right) = 1.05574 \text{ [cm}^{-1}] \quad (30)$$

We now address the choice of powers p_{ad} , q_{ad} , p_{na} and q_{na} for defining the radial expansion variables in Eqs. (27) and (28). As was pointed out in Ref. 21, if the effective adiabatic potential for the ‘minor’ isotopologues is to have the same limiting long-range behavior as that for the reference isotopologue, p_{ad} must be greater than or equal to the power of the longest-range term in the intermolecular potential for that state. Thus, we set $p_{\text{ad}}(a^3\Sigma_u^+) = 6$ and $p_{\text{ad}}(1^3\Sigma_g^+) = 3$. Note that BOB radial strength functions are relatively weak and slowly varying, and few terms are required to define them. As a result, there is no need here to introduce an $r_{\text{ref}} \neq r_e$ extension into the definition of the expansion variables in Eqs. (27) and (28), and for the sake of simplicity we set $q_{\text{ad}}(a^3\Sigma_u^+) = p_{\text{ad}}(a^3\Sigma_u^+) = 6$ and $q_{\text{ad}}(1^3\Sigma_g^+) = p_{\text{ad}}(1^3\Sigma_g^+) = 3$.

We are not aware of any theoretical predictions regarding the limiting long-range behavior of the centrifugal non-adiabatic radial strength function $\tilde{R}_{\text{ad}}^{\text{A}}(r)$, so we have no basis for assigning particular values to p_{na} . Moreover, as in the discussion of § III.B.(iii), there are no physical constraints on the values of q_{na} . At the same time, Fig. 3 of Ref. 22 shows that use of too small values for these powers can give rise to physically implausible extrema in the resulting functions on the interval between

the data region and the asymptote, while use of too high values will lead to a requirement for an excessive number of expansion coefficients. For simplicity, we therefore chose to set $p_{\text{na}} = q_{\text{na}} = 3$ in fits to models which included non-zero $\tilde{R}_{\text{na}}^{\text{Li}}(r)$ functions for either electronic state.

Since $y_{p_{\text{ad}}}^{\text{ref}}(r_e) = 0$ and $y_{p_{\text{ad}}}^{\text{ref}}(r \rightarrow \infty) = 1$, the algebraic form of Eq. (27) means that the difference between the well depths of different Li_2 isotopologues in a given electronic state is given by the expression¹⁰

$$\delta \mathfrak{D}_e^{(\alpha)} = \mathfrak{D}_e^{(\alpha)} - \mathfrak{D}_e^{(1)} = \left(\frac{\Delta M_{\text{Li}^a}^{(\alpha)}}{M_{\text{Li}^a}^{(\alpha)}} + \frac{\Delta M_{\text{Li}^b}^{(\alpha)}}{M_{\text{Li}^b}^{(\alpha)}} \right) (u_{\infty}^{\text{Li}} - u_0^{\text{Li}}), \quad (31)$$

and that the analogous shift in the equilibrium distance r_e is

$$\delta r_e^{(\alpha)} = r_e^{(\alpha)} - r_e^{(1)} = - \left(\frac{\Delta M_{\text{Li}^a}^{(\alpha)}}{M_{\text{Li}^a}^{(\alpha)}} + \frac{\Delta M_{\text{Li}^b}^{(\alpha)}}{M_{\text{Li}^b}^{(\alpha)}} \right) \frac{\tilde{S}'_{\text{ad}}(r_e)}{\bar{k}}, \quad (32)$$

in which \bar{k} is the harmonic force constant at the potential minimum in units $\text{cm}^{-1} \text{\AA}^2$, and

$$\tilde{S}'_{\text{ad}}(r_e) \equiv \left(\frac{d\tilde{S}_{\text{ad}}}{dr} \right)_{r=r_e} = \frac{(u_{\infty} - u_0)p_{\text{ad}} + u_1 q_{\text{ad}}}{2 r_e}. \quad (33)$$

Similarly, the electronic isotope shift will be

$$\begin{aligned} \delta \{ \Delta T_e^{(\alpha)} \} &= \Delta T_e^{(\alpha)} - \Delta T_e^{(1)} \\ &= \left(\frac{\Delta M_{\text{Li}^a}^{(\alpha)}}{M_{\text{Li}^a}^{(\alpha)}} + \frac{\Delta M_{\text{Li}^b}^{(\alpha)}}{M_{\text{Li}^b}^{(\alpha)}} \right) [u_0^{\text{Li}}(1^3\Sigma_g^+) - u_0^{\text{Li}}(a^3\Sigma_u^+)]. \end{aligned} \quad (34)$$

Note that in the present context, $\mathfrak{D}_e^{(1)}$ and $r_e^{(1)}$ are the values of the well depth and equilibrium distance of the MLR potential for the reference isotopologue species, and are determined by the DPF analysis.

Finally, as was pointed out by McAlexander *et al.*,⁴⁵ for the $1^3\Sigma_g^+$ state of Li_2 , the dominant BOB contribution to the rotationless potential at large r has the form

$$\Delta V_{\text{ad}}^{(\alpha)} \simeq 2 B^{(\alpha)}(r) = 2 \left(\frac{\hbar^2}{2\mu_{\alpha} r^2} \right), \quad (35)$$

and since μ_{α} for isotopic Li_2 is relatively small, this behavior must be considered. Following the approach of Refs. 10, 45, and 46, we have chosen to treat this term as a separate additive contribution to the effective interaction potential for each isotopologue, which therefore takes on the form:

$$V_{\text{ad,tot}}^{(\alpha)}(r) = V_{\text{MLR}}(r) + \Delta V_{\text{ad}}^{(\alpha)}(r) + 2 B^{(\alpha)}(r). \quad (36)$$

As was pointed out by Vogt *et al.*,⁴⁶ this $\Delta V_{\text{ad}}(r)$ term is readily incorporated into the Hamiltonian by simply replacing the factor $[J(J+1)]$ in Eq. (3) by $[J(J+1)+2]$, and their approach was adopted here. However, this means that the overall $1^3\Sigma_g^+$ -state well depth and equilibrium distance are actually $\mathfrak{D}_e^{\text{tot}}(c) = \mathfrak{D}_e^{(\alpha)} - 2 B^{(\alpha)}(r_e)$ and $r_e^{\text{tot}}(c) = r_e^{(\alpha)} + 4 B^{(\alpha)}(r_e)/(\bar{k} r_e)$, where $\mathfrak{D}_e^{(\alpha)}$ and $r_e^{(\alpha)}$ are defined by Eqs. (31) and (32), and $\mathfrak{D}_e^{(1)}$ and $r_e^{(1)}$ are the (fitted) reference-isotopologue MLR parameters for that state.

III. POTENTIALS FOR THE $a^3\Sigma_u^+$ AND $1^3\Sigma_g^+$ STATES OF Li_2

A. Data Set and Methodology

An overview of the experimental data used in this work is presented in Table I. Most of the data (2555 out of 2792 observations), came from fluorescence experiments performed by Martin *et al.*¹² and Linton *et al.*¹³ That data set was enlarged by inclusion of 137 $2^3\Pi_g - a^3\Sigma_u^+$ transitions of $^7,7\text{Li}_2$ taken from the study of Ref. 14, which extended the $a^3\Sigma_u^+$ vibrational range to $v = 9$. Finally, information about levels lying very near dissociation is provided by the one available PAS datum for the $v = 10$ level of the $a^3\Sigma_u^+$ state,¹⁵ and 99 PAS data for the higher levels of the $1^3\Sigma_g^+$ state.^{16,53} Throughout this study, the upper levels of all transitions originating in the $2^3\Pi_g$ state were represented by independent fitted term values. A listing of the experimental data used in the present analysis is included in the Supplementary Data supplied to the journal's www archive

All of the DPF data-analysis fits described herein were performed using the program DPotFit, which is freely available (with a manual) for download from the www.¹⁷ The initial trial values of the parameters β_i required for those fits were generated by applying the program betaFIT (also available from the www)¹⁸ to sets of turning points obtained from preliminary versions of the analysis.

B. Model for $\text{Li}_2(a^3\Sigma_u^+)$

The $a^3\Sigma_u^+$ state of Li_2 dissociates to yield two S -state atoms, and ignoring hyperfine effects, there is no noteworthy interstate coupling. The theory of intermolecular forces therefore tells us that the leading contributions to the long-range intermolecular potential should consist of terms associated with (inverse) powers $m_i = \{6, 8, 10\}$. The present analysis therefore represented the potential energy for this species by an MLR potential incorporating the long-range tail function

$$u_{\text{LR}}^{\{a^3\Sigma_u^+\}}(r) = D_6(r) \frac{C_6}{r^6} + D_8(r) \frac{C_8}{r^8} + D_{10}(r) \frac{C_{10}}{r^{10}} , \quad (37)$$

in which $D_m(r)$ are the modified Douketis-type damping functions of Eq. (13), $\rho = 0.54$,²⁴ and the dispersion energy coefficients for this state were fixed at the values reported by Tang *et al.*⁴²

In the initial work to determine an optimum model for this state, the PAS data for the $1^3\Sigma_g^+$ state were ignored and all of the observed levels of both the $1^3\Sigma_g^+$ and $2^3\Pi_g$ states were represented by independent term values, so only a single potential energy function was involved in the analysis. Fits were then performed to a wide variety of models corresponding to different choices for the order N of the polynomial in Eq. (14), and for the power q and the reference distance r_{ref} of Eq. (15). As was pointed out in § II.B, the power p must be larger than the difference between the largest and smallest powers of the terms contributing to Eq. (37), so it was fixed as $p = 5$.

Figure 5 summarizes results obtained for six families of potential function models of this type. For any given values of q and r_{ref} , the fits will always converge when the polynomial order N becomes sufficiently large. This point is illustrated by the convergence of the four families of solid triangular points shown in the lower panel of Fig. 5, which correspond to models with $q = 3$ and N increasing from two to five. The results for $N = 3$ with $q = 2$ and 4 (open square and round points, respectively) show that the optimum value of r_{ref} will depend on other features of the model, but convergence to the same limiting quality-of-fit \overline{dd} and essentially the same limiting values of

physically interesting parameters such as \mathfrak{D}_e will be achieved in any case. The upper panel of Fig. 5 shows the fitted values of \mathfrak{D}_e for the various models considered in the lower panel. Those results show that the fitted value of \mathfrak{D}_e may vary considerably from one model to another, but at the r_{ref} value where \overline{dd} approaches its minimum value, *all* models converge to essentially the same value of \mathfrak{D}_e .

All of the fits that are summarized by Fig. 5 used all of the 2693 ‘optical’ data for the two isotopologues $^{7,7}\text{Li}_2$ and $^{6,7}\text{Li}_2$, plus the one PAS datum which had been reported for the $a^3\Sigma_u^+$ state, while the 395 term values of the observed levels of the $1^3\Sigma_g^+$ state and 20 term values for the $2^3\Pi_g$ state were treated as free parameters. As might be expected when dealing with light atoms such as Li, BOB effects are not negligible in this system. In particular, it was found that allowing for one non-zero term u_0^{Li} in the expression for the ‘adiabatic’ correction radial strength function of Eq. (27) reduced the value of \overline{dd} by 2.4%; however, freeing a second coefficient (u_1^{Li}) only reduced \overline{dd} by an additional 0.08%, and the resulting value of u_1^{Li} had an uncertainty of greater than 100%. Similarly, allowing one centrifugal BOB parameter t_1^{Li} to vary led to reductions in \overline{dd} of less than 0.05%. As a result, the model actually used to obtain the results summarized in Fig. 5 included only the one free BOB parameter u_0^{Li} .

All else being equal, the “best” model for a given system is the one which achieves an optimum quality of fit (lowest \overline{dd}) with the smallest number of free parameters. When more than that minimum number of parameters are used, the additional degrees of freedom in parameter space will not be strongly constrained by the data, and the possibility of problems in the extrapolation regions tends to increase. On this basis we choose the M3LR $_{5,3}^{8,0}(3)$ model corresponding to the ‘gradient-shaped’ black points at $r_{\text{ref}} = 8.0 \text{ \AA}$ on Fig. 5 as our preferred model. To four decimal places, increasing N by one had no effect on the associated value of $\overline{dd} = 0.7069$. While the analysis described above led to our determination of optimal models for the $a^3\Sigma_u^+$ -state potential and BOB function, the associated parameters were also allowed to vary freely in the global two-state fit which simultaneously determined potential energy functions for the $1^3\Sigma_g^+$ state. Hence, they will be reported later.

One final component of this discussion is an illustration of the remarkably robust extrapolation properties of the MLR potential form. In the initial stages of this study, only the optical $1^3\Sigma_g^+ - a^3\Sigma_u^+$ data which spanned vibrational levels $v(a) = 0 - 7$ were considered in the analysis. The highest of the associated $a^3\Sigma_u^+$ -state levels is bound by 26 cm^{-1} for $^{7,7}\text{Li}_2$ and by 16 cm^{-1} for $^{6,6}\text{Li}_2$. Nonetheless, the optimal MLR potential obtained from that analysis was an M3LR $_{5,3}^{8,0}(r)$ function whose well depth of $\mathfrak{D}_e = 333.79(1) \text{ cm}^{-1}$ is very close to the value $333.76(1) \text{ cm}^{-1}$ yielded by the analysis of the full $a^3\Sigma_u^+$ -state data set (see Fig. 5). Moreover, the $v(a) = 10$ binding energy predicted by that potential was 0.4222 cm^{-1} , which is remarkably close to the measured PAS value¹⁵ of $0.4160(\pm 0.0013) \text{ cm}^{-1}$. Thus, a DPF analysis using an MLR potential with a good multi-term theoretical $u_{\text{LR}}(r)$ seems capable of yielding quite reliable extrapolations to predict both the distance from the highest observed level to dissociation and the number and energies of unobserved higher levels.

C. Model for $\text{Li}_2(1^3\Sigma_g^+)$ and Results of the Two-State Analysis

Following the discussion of § II.C, the potential energy function for the $1^3\Sigma_g^+$ state of Li_2 was represented by an MLR potential whose long-range tail was defined by $u_{\text{LR}}^{\text{ret}}(r)$ of Eq. (26). As usual, fits were performed using models corresponding to a variety of values of the exponent polynomial order N , of the power q defining the polynomial expansion variable, and of the reference distance r_{ref} of Eq. (15). Since the inverse-power terms contributing to $u_{\text{LR}}^{\text{ret}}(r)$ have powers $m_i = \{3, 6, 8\}$, the power p defining the radial variables $y_p^{\text{eq}}(r)$ and $y_p^{\text{ref}}(r)$ of Eqs. (8) and (15) was fixed at $p = 6$ ($> 8 - 3$), and while C_6^Σ and C_8^Σ were held fixed at the theoretical values of Tang *et al.*,⁴² C_3^Σ was treated as a free parameter. All of these fits treated the full range of data for the $1^3\Sigma_g^+ - a^3\Sigma_u^+$ system, and while the potential for the $a^3\Sigma_u^+$ state was represented by the $\text{M3LR}_{5,3}^{8,0}(r)$ model described in § III.B, its parameters were also free variables in these fits.

Figure 6 summarizes results for six families of $1^3\Sigma_g^+$ -state PECs: those for exponent polynomial orders $N = 6 - 9$ with $q = 3$ being represented by solid points, while those for polynomials orders $N = 8 - 9$ with $q = 4$ (bottom panel only) are shown as open points. As is expected, the fact that the 395 observed $1^3\Sigma_g^+$ -state level energies are now constrained to be eigenvalues of a potential function rather than being free fitting parameters means that the \overline{dd} values associated with the best of these fits are somewhat larger than those for the $a^3\Sigma_u^+$ -state analyses summarized in Fig. 5.

As has been the case in other treatments of this type, for any reasonable values of q and r_{ref} the fits converge to essentially the same optimum \overline{dd} value when the polynomial order N becomes sufficiently large.^{10,24,32,47,48} A manual optimization of r_{ref} is undertaken in order to determine a ‘best’ model, which is defined as one which: (i) gives a good fit to all data, (ii) is defined by the smallest number of free parameters, and (iii) has no unphysical behavior in the extrapolation regions. As is usually the case, models with larger q values (here $q=4$) require a higher-order polynomial to achieve a given quality of fit. While not shown, the \overline{dd} values for $N = 10$, $q = 4$ models with $r_{\text{ref}} = 3.4 - 3.6$ are essentially identical to those for $N = 9$, $q = 3$ models with the same r_{ref} (solid round points), but are bigger at larger and smaller r_{ref} values. Models with $q = 1$ or 2 tended to have inflection points on the short-range repulsive wall, even for cases with fairly large r_{ref} values.

The results in the two upper panels of Fig. 6 show that the values of \mathfrak{D}_e and C_3^Σ yielded by fits to models with $N = 9$, $q = 3$ vary relatively slowly with r_{ref} , and that for r_{ref} values which give small \overline{dd} values, other types of models yield very similar results. For both of these properties the analogous results for $q = 4$ models were much more strongly model-dependent. We therefore chose the $N = 9$, $q = 3$ potential with $r_{\text{ref}} = 3.6 \text{ \AA}$ as our recommended model for this state.

The error bars shown in Fig. 6 are the 95% confidence limit uncertainties in the parameter yielded by the non-linear least-squares fits. Although the binding energies of the highest observed levels for the $1^3\Sigma_g^+$ state are even smaller than was the case for the $A^1\Sigma_u^+$ state,¹⁶ the uncertainties in the fitted C_3^Σ values obtained here ($\gtrsim 75 \text{ cm}^{-1} \text{ \AA}^3$) are an order of magnitude larger than the analogous uncertainties yielded by the $A - X$ analysis of Ref. 10. It is not clear why this should be the case, other than the fact that the data gap from $v(1^3\Sigma_g^+) = 8$ to 61 for $^7,^7\text{Li}_2$ or to 55 for $^6,^6\text{Li}_2$ may be expected to introduce additional uncertainty into the analysis of the limiting near-dissociation behavior. However, the difference between the C_3^Σ value implied by the present analysis and that

determined from the $A - X$ analysis of Ref. 10 (dash-dot-dot line in the uppermost panel of Fig. 6) is significantly larger than the mutual uncertainties. Moreover, repeating the present analysis with C_3^Σ fixed at the value yielded by the $A - X$ analysis ($357\,829(\pm 8)\text{ cm}^{-1}\text{ \AA}^3$) increased the overall value of \overline{dd} by 0.8%, and increased \overline{dd} for the PAS data by a massive 21%! It may be that a combined 5-state analysis of the data sets for the two cases will resolve this discrepancy, but that is beyond the scope of the present work. Thus, our recommended model for the $1^3\Sigma_g^+$ state is an M3LR_{6,3}^{3,6}(9) potential with $u_{\text{LR}}(r)$ defined by Eq. (26), and with C_3^Σ determined from the fit.

The parameters defining our recommended models for the $a^3\Sigma_u^+$ and $1^3\Sigma_g^+$ states of Li_2 are listed in Table II. The fact that the uncertainties in the values of \mathfrak{D}_e and r_e are an order of magnitude larger for the $1^3\Sigma_g^+$ state is to be expected, both because of the 5200 cm^{-1} data gap for $v > 7$, and because the fact that its lowest observed level is $v = 1$ means that the extrapolation to the potential minimum is much longer for this case. As for the $a^3\Sigma_u^+$ state, obtaining a good combined-isotopologue fit required the introduction of BOB corrections in the effective adiabatic potential function for the $1^3\Sigma_g^+$ state. As shown in Table II, our recommended model includes a third-order polynomial expression for the ‘adiabatic’ correction radial strength function $\tilde{S}_{\text{ad}}^{\text{Li}}(r)$. Increasing this polynomial order further or allowing for a non-zero centrifugal BOB function yielded no significant improvement in the quality of fit, while reducing this polynomial order by one or two terms increased the \overline{dd} value for the fit by 1.6% or 3.8%, respectively.

D. BOB Functions and Isotope Effects

The radial strength functions defining the effective adiabatic BOB correction to the potential energy functions for both states are shown in Fig. 7. Since $^{7,7}\text{Li}_2$ was chosen as the reference isotopologue, Eq. (31) shows that the fact that $\tilde{S}_{\text{ad}}^{\{a^3\Sigma_u^+\}}(r_e^{\{a^3\Sigma_u^+\}}) - \tilde{S}_{\text{ad}}^{\{a^3\Sigma_u^+\}}(\infty) = u_0^{\{a^3\Sigma_u^+\}} - u_\infty^{\{a^3\Sigma_u^+\}} = u_0^{\{a^3\Sigma_u^+\}}$ is positive means that $\mathfrak{D}_e^{\{a^3\Sigma_u^+\}}$ is (slightly) larger for $^{6,6}\text{Li}_2$ than for $^{7,7}\text{Li}_2$. The upper curve in Fig. 7 shows that the $\tilde{S}_{\text{ad}}^{\{1^3\Sigma_g^+\}}(r)$ contribution to the isotopologue dependence of $\mathfrak{D}_e^{\{1^3\Sigma_g^+\}}$ is also positive (and much larger). However, the isotopologue dependence of the $2B^{(\alpha)}(r)$ contribution to the effective adiabatic potential (see Eq. (36)) makes a negative (-0.171 cm^{-1}) contribution to the difference $\mathfrak{D}_e^{\text{tot}(6,6)} - \mathfrak{D}_e^{\text{tot}(7,7)}$ for the $1^3\Sigma_g^+$ state, and turns out to be the dominant term.

The results presented in Table II were obtained from an analysis which treated $^{7,7}\text{Li}_2$ as the reference isotopologue, and the first row of Table III presents characteristic properties of the resulting $a^3\Sigma_u^+$ and $1^3\Sigma_g^+$ potential energy functions for that species. Note that the values of $\mathfrak{D}_e^{\text{tot}}(1^3\Sigma_g^+)$ and $r_e^{\text{tot}}(1^3\Sigma_g^+)$ were obtained after combining the MLR potential with the additive adiabatic correction term of Eq. (35). The next two rows of this table then show, respectively, the isotopic changes in and the resulting values of these quantities for $^{6,6}\text{Li}_2$, as implied by the BOB correction functions $\tilde{S}_{\text{ad}}(r)$ and (for the $1^3\Sigma_g^+$ state) the $2B^{(\alpha)}(r)$ term (see Eqs. (31)–(36)). Of course it is equally feasible to perform the overall analysis using $^{6,6}\text{Li}_2$ as the reference isotopologue, and the last row of Table III shows the properties of that isotopologue obtained in that more direct manner. It is reassuring to see that within the uncertainties, the results in the last two rows of this table agree with one another.

Of course it is simpler to work with potential functions that do not require the addition of separate adiabatic correction functions $\Delta V_{\text{ad}}^{(\alpha)}(r)$. Hence, for the convenience of those interested primarily

in the minor isotopologue ${}^6\text{Li}_2$, a version of Table II for the case in which this species was used as the reference isotopologue is included in the Supplementary Data supplied to the journal’s www archive.

IV. DISCUSSION AND CONCLUSIONS

A combined-isotopologue DPF analysis of 2692 optical data for the $1^3\Sigma_g^+ - a^3\Sigma_u^+$ and $2^3\Pi_g - a^3\Sigma_u^+$ band systems of ${}^{7,7}\text{Li}_2$ and ${}^{6,6}\text{Li}_2$, together with 99 PAS data for the $1^3\Sigma_g^+$ state and one for the $a^3\Sigma_u^+$ state, has yielded analytic potential energy functions for the $1^3\Sigma_g^+$ and $a^3\Sigma_u^+$ electronic states which (on average) explain all of those data within the experimental uncertainties ($\overline{dd} = 0.789$). The present potential energy function for the $a^3\Sigma_u^+$ state of Li_2 is one of the most accurate ground-triplet-state potentials determined for any alkali-atom pair. The resulting scattering lengths for ${}^{7,7}\text{Li}_2$ and ${}^{6,6}\text{Li}_2$ are $a_{\text{SL}} = -14.759(9) \text{ \AA}$ and $-1906(50) \text{ \AA}$, respectively, where the uncertainties were estimated by repeating the overall analysis with $C_6^{\{a^3\Sigma_g^+\}}$ increased/decreased by 0.01% from the recommended values of Tang *et al.*⁴² This 0.01% is a factor of 3 larger than the C_6 uncertainty reported in Ref. 42. The uncertainty in a_{SL} is much larger for ${}^{6,6}\text{Li}_2$ than for ${}^{7,7}\text{Li}_2$ simply because all else being equal, scattering lengths that are very large in magnitude are much more sensitive to details of the potential energy function. Listings of band constants (G_v , B_v , D_v , H_v , etc.) calculated from this potential for all bound levels of the $a^3\Sigma_u^+$ state for all three Li_2 isotopologues are included with the Supplementary Data supplied to the journal’s www archive.

For the $1^3\Sigma_g^+$ state, the present analysis has provided an analytic potential energy function which very robustly bridges the $\sim 5200 \text{ cm}^{-1}$ gap shown in Fig. 1, between the fluorescence measurement domain $v = 1 - 7$ and the PAS data for $v \geq 56$ for ${}^{6,6}\text{Li}_2$ and ≥ 62 for ${}^{7,7}\text{Li}_2$. To illustrate this interpolation behavior, Fig. 8 plots calculated properties of our recommended potential for ${}^{7,7}\text{Li}_2$ in the manner suggested by near-dissociation theory (NDT).^{47,49–52} In particular, NDT predicts that for vibrational levels lying near the dissociation limit of a potential whose limiting long-range behavior is defined by an attractive C_3/r^3 interaction energy, the $1/6$ power of the binding energy ($\mathfrak{D} - E_v$), the $1/5$ power of the vibrational level spacing $\Delta G_{v+1/2}$, and the $1/4$ power of the inertial rotational constant B_v , should all be linear functions of v , with slopes determined by the value of the C_3 coefficient. The solid triangular points in Fig. 8 represent the experimental data, while the open round points are our predictions for the ‘no-data’ regions. The dash-dot-dot lines in Fig. 6 are the limiting NDT slopes implied by the fitted C_3^Σ value of Table II. The deviation from this behavior at very high v reflects the fact that the 3×3 interstate coupling reduces the magnitude of the effective C_3 coefficient in the limiting region by a factor of $1/3$ (see Fig. 4) as one approaches the limit. Calculated band constants for all bound levels of all three Li_2 isotopologues in this state have been placed in the journal’s Supplementary Data archive.

It is noteworthy that predictions generated from a variety of other MLR potential models (i.e., models defined by different N or q values) which yield good fits to the data are identical on the scale of Fig. 8. This model-independent bridging of a data-gap spanning 73% of the well depth is a remarkable illustration of the robustness of the MLR potential function form. The ability of this function to readily incorporate the effect of two-state¹⁰ or three-state (present work) coupling

in the long-range region is a further demonstration of its capabilities. A FORTRAN subroutine for generating the recommended potentials is one of the items placed in the journal’s Supplementary Data archive.

One puzzle left by this work is the discrepancy between the value of C_3^Σ for interacting $\text{Li}(^2P) + \text{Li}(^2S)$ atoms determined in the present analysis ($3.575\,57(78) \times 10^5 \text{ cm}^{-1} \text{ \AA}^3$) and those obtained in the $A(^1\Sigma_u^+)$ -state analysis of Ref. 10 ($3.578\,29(7) \times 10^5 \text{ cm}^{-1} \text{ \AA}^3$) or from the recent theoretical calculations of Tang *et al.*,⁴² ($3.578\,108\,9(7) \times 10^5 \text{ cm}^{-1} \text{ \AA}^3$). While small on an absolute scale, this 0.076% discrepancy is much larger than the estimated uncertainties, and repeating our overall analysis with C_3^Σ fixed at the A -state value from Ref. 10 yielded a distinctly poorer quality fit, especially for the PAS data. It may be that a combined five-state analysis of all of the data considered here with those used in the $A - X$ analysis of Ref. 10 will shed light on this question, but that will have to await future work.

Acknowledgements

We are very grateful to Dr. Amanda Ross for stimulating discussions which brought this problem to our attention, and to Professor F.R.W. McCourt for helpful discussions. This research has been supported by the Natural Sciences and Engineering Research Council of Canada.

-
- ¹ D. K. Hsu, *The Absorption Spectra of the $A - X$ and $C - X$ Transitions of the ($^7\text{Li}_2$) Lithium Molecule*, Ph.D. Dissertation, Fordham University (1975).
 - ² B. Barakat, R. Bacis, F. Carrot, S. Churassy, P. Crozet, F. Martin, and J. Vergès, *Chem. Phys.* **102**, 215 (1986).
 - ³ K. Urbanskiand, S. Antonova, A. Yiannopoulou, A. M. Lyyra, L. Li, and W. C. Stwalley, *J. Chem. Phys.* **104**, 2813 (1996), erratum, *ibid* **116**, 10557 (2002).
 - ⁴ C. Linton, F. Martin, I. Russier, A. J. Ross, P. Crozet, S. Churassy, and R. Bacis, *J. Mol. Spectrosc.* **175**, 340 (1996).
 - ⁵ F. Martin, M. Aubert-Frécon, R. Bacis, P. Crozet, C. Linton, S. Magnier, A. Ross, and I. Russier, *Phys. Rev. A* **55**, 3458 (1997).
 - ⁶ X. Wang, J. Yang, J. Qi, and A. M. Lyyra, *J. Mol. Spectrosc.* **191**, 295 (1998).
 - ⁷ X. Wang, J. Magnes, A. M. Lyyra, A. J. Ross, F. Martin, P. M. Dove, and R. J. Le Roy, *J. Chem. Phys.* **117**, 9339 (2002).
 - ⁸ A. Adohi-Krou, F. Martin, A. J. Ross, C. Linton, and R. J. Le Roy, *J. Chem. Phys.* **121**, 6309 (2004).
 - ⁹ J. A. Coxon and T. C. Melville, *J. Mol. Spectrosc.* **235**, 235 (2006).
 - ¹⁰ R. J. Le Roy, N. Dattani, J. A. Coxon, A. J. Ross, P. Crozet, and C. Linton, *J. Chem. Phys.* **131**, 204309 (2009).
 - ¹¹ X. Xie and R. W. Field, *J. Chem. Phys.* **83**, 6193 (1985).

- ¹² F. Martin, R. Bacis, J. Vergés, C. Linton, G. Bujin, C. H. Cheng, and E. Stad, *Spectrochim. Acta A* **44**, 1369 (1988).
- ¹³ C. Linton, T. L. Murphy, F. Martin, R. Bacis, and J. Verges, *J. Chem. Phys.* **91**, 6036 (1989).
- ¹⁴ C. Linton, F. Martin, A. J. Ross, I. Russier, P. Crozet, A. Yiannopoulou, L. Li, and A. M. Lyyra, *J. Mol. Spectrosc.* **196**, 20 (1999).
- ¹⁵ E. R. I. Abraham, W. I. McAlexander, C. A. Sackett, and R. G. Hulet, *Phys. Rev. Lett.* **74**, 1315 (1995).
- ¹⁶ E. R. I. Abraham, N. W. M. Ritchie, W. I. McAlexander, and R. G. Hulet, *J. Chem. Phys.* **103**, 7773 (1995).
- ¹⁷ R. J. Le Roy, J. Seto, and Y. Huang, *DPotFit 1.2: A Computer Program for fitting Diatomic Molecule Spectra to Potential Energy Functions*, University of Waterloo Chemical Physics Research Report CP-664 (2007); see <http://leroy.uwaterloo.ca/programs/>.
- ¹⁸ R. J. Le Roy, *betaFIT 2.0: A Computer Program to Fit Potential Function Points to Selected Analytic Functions*, University of Waterloo Chemical Physics Research Report CP-665 (2009); see <http://leroy.uwaterloo.ca/programs/>.
- ¹⁹ J. K. G. Watson, *J. Mol. Spectrosc.* **80**, 411 (1980).
- ²⁰ J. K. G. Watson, *J. Mol. Spectrosc.* **223**, 39 (2004).
- ²¹ R. J. Le Roy, *J. Mol. Spectrosc.* **194**, 189 (1999).
- ²² R. J. Le Roy and Y. Huang, *J. Mol. Struct. (Theochem)* **591**, 175 (2002).
- ²³ Y. Huang and R. J. Le Roy, *J. Chem. Phys.* **119**, 7398 (2003); erratum: *ibid* **126** 169904 (2007).
- ²⁴ R. J. Le Roy, C. C. Haugen, J. Tao, and H. Li, *Mol. Phys.* **109**, xxxx (2011, in press).
- ²⁵ H. Margenau, *Rev. Mod. Phys.* **11**, 1 (1939).
- ²⁶ J. O. Hirschfelder, C. F. Curtiss, and R. B. Bird, *Molecular Theory of Gases and Liquids* (Wiley, New York, 1964).
- ²⁷ J. O. Hirschfelder and W. J. Meath, in *Intermolecular Forces*, Vol. 12 of *Adv. Chem. Phys.*, edited by J. O. Hirschfelder (Interscience, New York, 1967), Chap. 1, pp. 3–106.
- ²⁸ G. C. Maitland, M. Rigby, E. B. Smith, and W. A. Wakeham, *Intermolecular Forces - Their Origin and Determination* (Oxford University Press, Oxford, UK, 1981).
- ²⁹ H. Kreek and W. J. Meath, *J. Chem. Phys.* **50**, 2289 (1969).
- ³⁰ C. Douketis, G. Scoles, S. Marchetti, M. Zen, and A. J. Thakkar, *J. Chem. Phys.* **76**, 3057 (1982).
- ³¹ R. J. Le Roy and R. D. E. Henderson, *Mol. Phys.* **105**, 663 (2007).
- ³² J. A. Coxon and P. G. Hajigeorgiou, *J. Chem. Phys.* **132**, 094105 (2010).
- ³³ R. J. Le Roy, Y. Huang, and C. Jary, *J. Chem. Phys.* **125**, 164310/1 (2006).
- ³⁴ H. Salami, A. J. Ross, P. Crozet, W. Jastrzebski, P. Kowalczyk, and R. J. Le Roy, *J. Chem. Phys.* **126**, 194313/1 (2007).
- ³⁵ F. Xie, V. B. Sovkov, A. M. Lyyra, D. Li, S. Ingram, J. Bai, V. S. Ivanov, S. Magnier, and L. Li, *J. Chem. Phys.* **130**, 051102 (2009).
- ³⁶ M. Movre and G. Pichler, *J. Phys. B: At. Mol. Phys.* **10**, 2631 (1977).
- ³⁷ M. Aubert-Frécon, G. Hadinger, S. Magnier, and S. Rousseau, *J. Mol. Spectrosc.* **188**, 182 (1998).
- ³⁸ C. J. Sansonetti, B. Richou, R. Engleman Jr., and L. J. Radziemski, *Phys. Rev. A* **52**, 2682 (1995).

- ³⁹ G. Cardano, *Ars Magna* (1545).
- ⁴⁰ J. Kopp, Int. J. Mod. Phys. C **19**, 523 (2008).
- ⁴¹ C. G. J. Jacobi, J. für die Reine und Angew. Math. **30**, 51 (1846).
- ⁴² L.-Y. Tang, Z.-C.-Yan, T.-Y. Shi, and J. F. Babb, Phys. Rev. A **79**, 062712 (2009).
- ⁴³ R. McLone and E. Power, Mathematica **II**, 91 (1964).
- ⁴⁴ W. J. Meath, J. Chem. Phys. **48**, 227 (1968).
- ⁴⁵ W. I. McAlexander, E. R. I. Abraham, and R. G. Hulet, Phys. Rev. A **54**, R5 (1996).
- ⁴⁶ F. Vogt, C. Grain, T. Nazarova, U. Sterr, F. Riehle, C. Lisdat, and E. Tiemann, Eur. Phys. J. D **44**, 73 (2007).
- ⁴⁷ R. J. Le Roy, *Determining Equilibrium Structures and Potential Energy Functions for Diatomic Molecules*, Chapter 6, pp.168-211, of *Equilibrium Structures of Molecules*, J. Demaison and A. G. Csaszar editors, Taylor & Francis, London (2010).
- ⁴⁸ R. D. E. Henderson, A. Shayesteh, J. Tao, C. C. Haugen, P. F. Bernath, and R. J. Le Roy, J. Chem. Phys. **XXX**, xxx (2011).
- ⁴⁹ R. J. Le Roy and R. B. Bernstein, Chem. Phys. Lett. **5**, 42 (1970).
- ⁵⁰ R. J. Le Roy and R. B. Bernstein, J. Chem. Phys. **52**, 3869 (1970).
- ⁵¹ R. J. Le Roy, Can. J. Phys. **50**, 953 (1972).
- ⁵² R. J. Le Roy, in *Semiclassical Methods in Molecular Scattering and Spectroscopy*, Vol. 53 of *Series C - Mathematical and Physical Sciences*, edited by M. Child (D. Reidel, Dordrecht, 1980), pp. 109–126.
- ⁵³ Three PAS data, those for $v(^{7,7}\text{Li}_2) = 62$, $N = 1$), $v(^{6,6}\text{Li}_2) = 80$, $N = 1$) and $v(^{6,6}\text{Li}_2) = 68$, $N = 2$) proved to be outliers, and were omitted from the final fits.

Table I: Summary of experimental data used in the present work.

isotop.	type	unc. (cm^{-1})	$v(2^3\Pi_g)$	$v(1^3\Sigma_g^+)$	$v(a^3\Sigma_u^+)$	# data	source
$^{7,7}\text{Li}_2$	$1^3\Sigma_g^+$ emission	0.01	—	1 – 7	0 – 7	1279	Ref. 12
	$2^3\Pi_g$ emission	0.005 – 0.01	1 – 2	—	0 – 9	137	Ref. 14
	PAS($1^3\Sigma_g^+$)	0.0043 – 0.00073	—	63 – 90	—	30	Ref. 16
	PAS($a^3\Sigma_u^+$)	0.0013	—	—	10	1	Ref. 15
$^{6,6}\text{Li}_2$	$1^3\Sigma_g^+$ emission	0.01	—	1 – 7	0 – 7	1276	Refs. 13
	PAS($1^3\Sigma_g^+$)	0.00110 – 0.01067	—	56 – 84	—	69	Ref. 16
Overall			1 – 2	1 – 90	0 – 10	2792	

Table II: Parameters defining the recommended MLR potentials and BOB functions for the $a^3\Sigma_u^+$ and $1^3\Sigma_g^+$ states of Li_2 obtained using $^7,^7\text{Li}_2$ as the reference isotopologue. Parameters in square brackets were held fixed in the fit, while numbers in round brackets are 95% confidence limit uncertainties in units of the last digits show. The analysis used the $^7\text{Li } ^2P_{1/2} \leftarrow 2S_{1/2}$ excitation energy of $14903.648130 \text{ cm}^{-1}$ and $^2P_{3/2} \leftarrow 2P_{1/2}$ spin-orbit splitting energy of 0.335338 cm^{-1} from Ref. 38. Units of length and energy are Å and cm^{-1} ; the exponent expansion coefficients β_i are dimensionless, while the parameters u_i defining the ‘adiabatic’ BOB strength function of Eq. (27) have units cm^{-1} .

	$a(^3\Sigma_u^+)$	$c(1^3\Sigma_g^+)$
\mathcal{D}_e	333.758 (7)	7093.44 (3)
r_e	4.17005 (3)	3.06514 (9)
C_6	$[6.7185 \times 10^6]$	C_3 $3.57557 (78) \times 10^5$
C_8	$[1.12629 \times 10^8]$	C_6^Σ $[1.00054 \times 10^7]$
C_{10}	$[2.78683 \times 10^9]$	C_8^Σ $[3.69953 \times 10^8]$
ρ_{Li}	$[0.54]$	N/A
$\{p, q\}$	$\{5, 3\}$	$\{6, 3\}$
r_{ref}	$[8.0]$	$[3.6]$
β_0	-0.51608	-1.6373863
β_1	-0.09782	0.29197
β_2	0.1137	-0.55544
β_3	-0.0248	-0.2794
β_4	—	-1.5993
β_5	—	-0.673
β_6	—	-1.23
β_7	—	-1.29
β_8	—	0.5
β_9	—	2.6
$\{p_{\text{ad}}, q_{\text{ad}}\}$	$\{6, 6\}$	$\{3, 3\}$
u_0	0.059 (11)	1.367 (7)
u_1	—	2.7 (4)
u_2	—	-1.3 (5)
u_3	—	-1.8 (4)
u_∞	$[0.0]$	$[1.055740]$

Table II.B: (for Supplementary Data submission)

Parameters defining the recommended MLR potentials and BOB functions for the $a\ ^3\Sigma_u^+$ and $1\ ^3\Sigma_g^+$ states of Li_2 obtained using $^6,^6\text{Li}_2$ as the reference isotopologue. Parameters in square brackets were held fixed in the fits, while numbers in round brackets are the 95% confidence limit uncertainties in units of the last digits show. The analysis used the $^6\text{Li}\ ^2P_{1/2} \leftarrow 2S_{1/2}$ excitation energy of $14903.296792\text{ cm}^{-1}$ and $^2P_{3/2} \leftarrow 2P_{1/2}$ spin-orbit splitting energy of 0.335324 cm^{-1} from Ref. 38. Units of length and energy are Å and cm^{-1} ; the exponent expansion coefficients β_i are dimensionless, while the parameters u_i defining the ‘adiabatic’ BOB strength function of Eq. (27) have units cm^{-1} .

	$a(^3\Sigma_u^+)$	$c(1\ ^3\Sigma_g^+)$
\mathfrak{D}_e	333.778 (7)	7093.54 (3)
r_e	4.17001 (3)	3.06520 (9)
C_6	$[6.7190 \times 10^6]$	C_3 $3.57549 (78) \times 10^5$
C_8	$[1.12634 \times 10^8]$	C_6^Σ $[1.00059 \times 10^7]$
C_{10}	$[2.78694 \times 10^9]$	C_8^Σ $[3.69965 \times 10^8]$
ρ_{Li}	$[0.54]$	N/A
$\{p, q\}$	$\{5, 3\}$	$\{6, 3\}$
r_{ref}	$[8.0]$	$[3.6]$
β_0	-0.516086	-1.6373493
β_1	-0.09783	0.29191
β_2	0.1136	-0.55591
β_3	-0.0249	-0.2788
β_4	—	-1.5931
β_5	—	-0.685
β_6	—	-1.306
β_7	—	-1.34
β_8	—	0.6
β_9	—	2.7
$\{p_{\text{ad}}, q_{\text{ad}}\}$	$\{6, 6\}$	$\{3, 3\}$
u_0	0.067 (13)	1.595 (8)
u_1	—	3.1 (5)
u_2	—	-1.5 (5)
u_3	—	-2.1 (5)
u_∞	$[0.0]$	$[1.23141]$

Table III: Properties of the recommended potential energy functions for the $a^3\Sigma_u^+$ and $1^3\Sigma_g^+$ states of Li_2 (energies in cm^{-1} and lengths in \AA), with ‘*changes*’ calculated using Eqs. (31)–(36). The first three rows correspond to use of $^7,^7\text{Li}_2$ as the reference isotopologue, while for the last row it was $^6,^6\text{Li}_2$.

fit	isot.	$a^3\Sigma_u^+$ state		ΔT_e	$1^3\Sigma_g^+$ state	
		\mathfrak{D}_e	r_e		$\mathfrak{D}_e^{\text{tot}}$	r_e^{tot}
2-isot	$^7,^7\text{Li}_2$	333.758(7)	4.17005(3)	8144.989(43)	7092.417(33)	3.06524(9)
	<i>change</i>	0.019(4)	−0.000015(3)	− 0.265(5)	−0.067(2)	0.000075(1)
	$^6,^6\text{Li}_2$	333.777(8)	4.17003 ₅ (3)	8144.724(43)	7092.349(33)	3.06532(9)
2-isot	$^6,^6\text{Li}_2$	333.778(7)	4.17001(3)	8144.726(33)	7092.347(33)	3.06532(9)

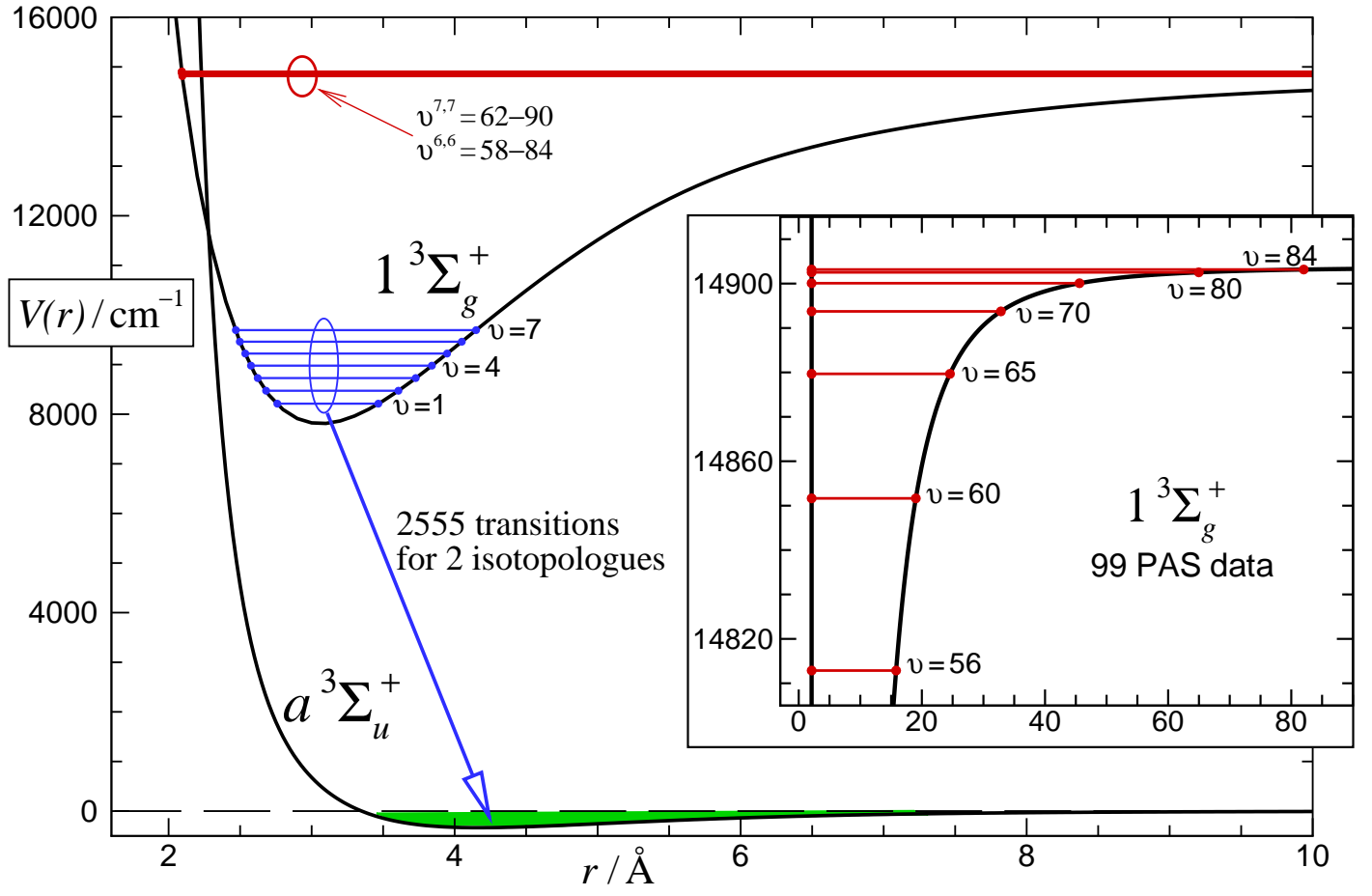


Figure 1.: Overview of the potential energy functions and observed vibrational levels of the $1^3\Sigma_g^+$ and $a^3\Sigma_u^+$ states associated with the present analysis. The insert shows a fragment of the $1^3\Sigma_g^+$ state potential at the energy range associated with the $^{6,6}\text{Li}_2$ PAS data.

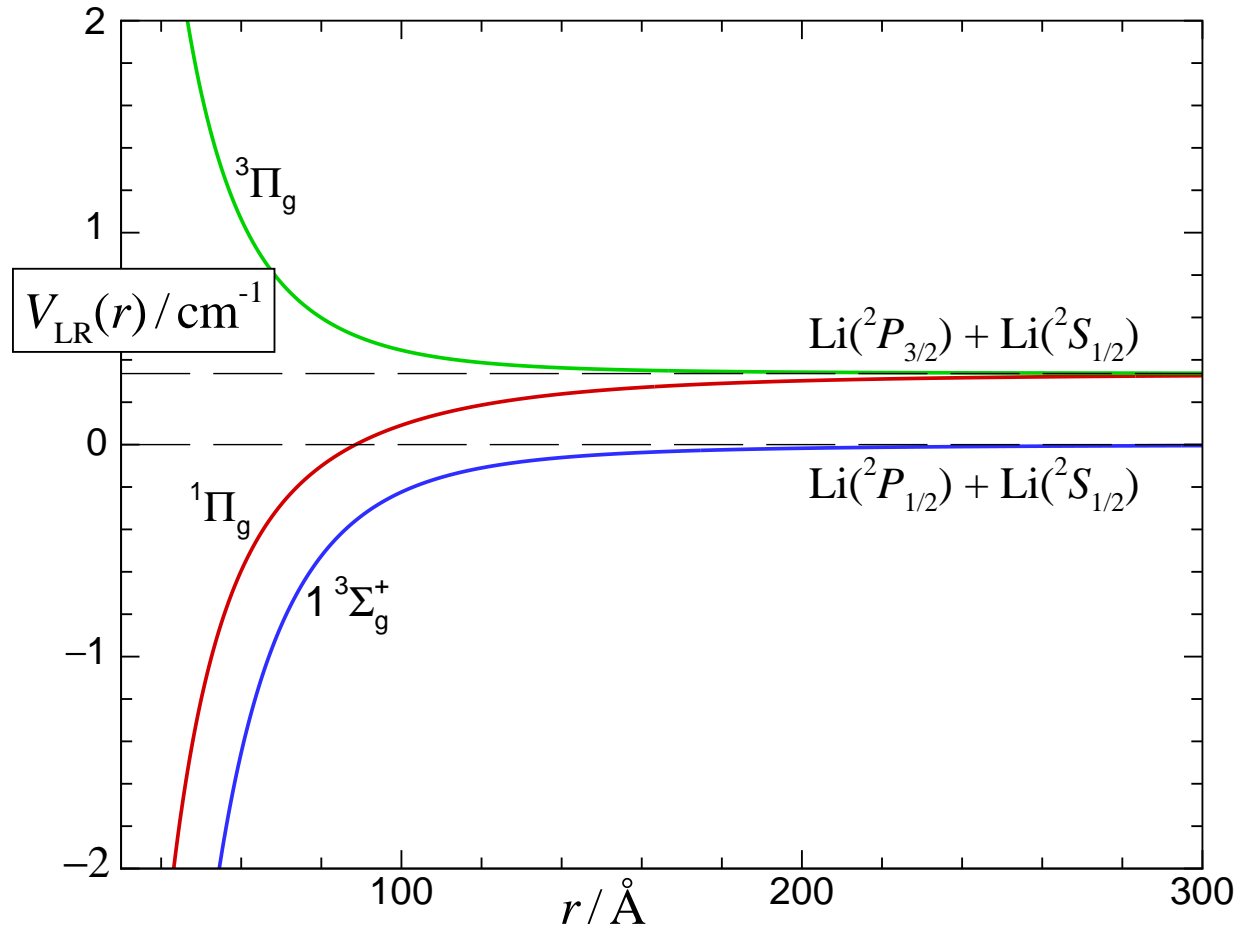


Figure 2.: Eigenvalues of Eq. (18) for the 1_g states of Li_2 dissociating to the $\text{Li}(2s^2S) + \text{Li}(2p^2P)$ limits, as generated using the long-range coefficients of Tang *et al.*⁴²

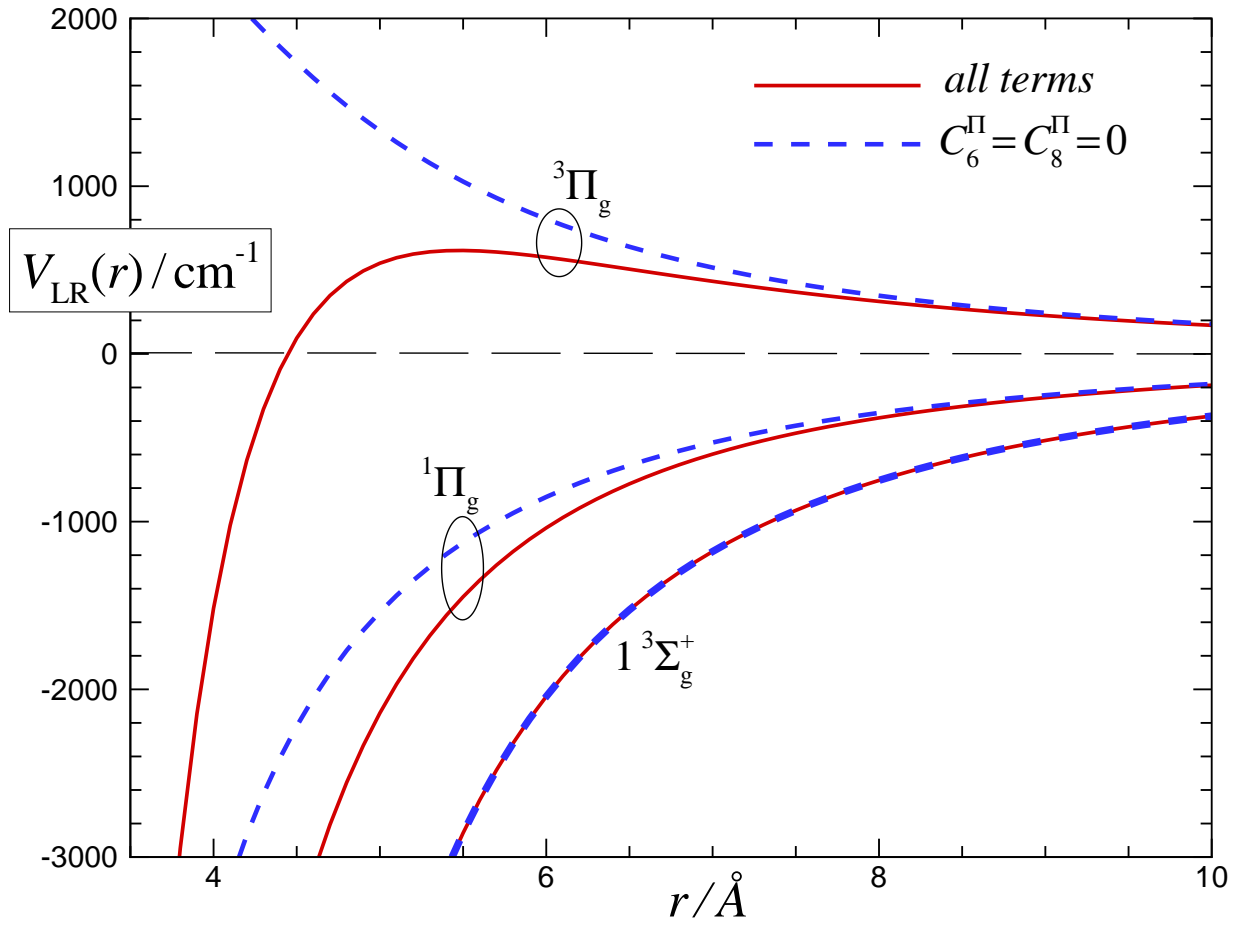


Figure 3.: Illustration of the effect of setting $C_6^\Pi = C_8^{1\Pi_g} = C_8^{3\Pi_g} = 0$ in Eq. (18).

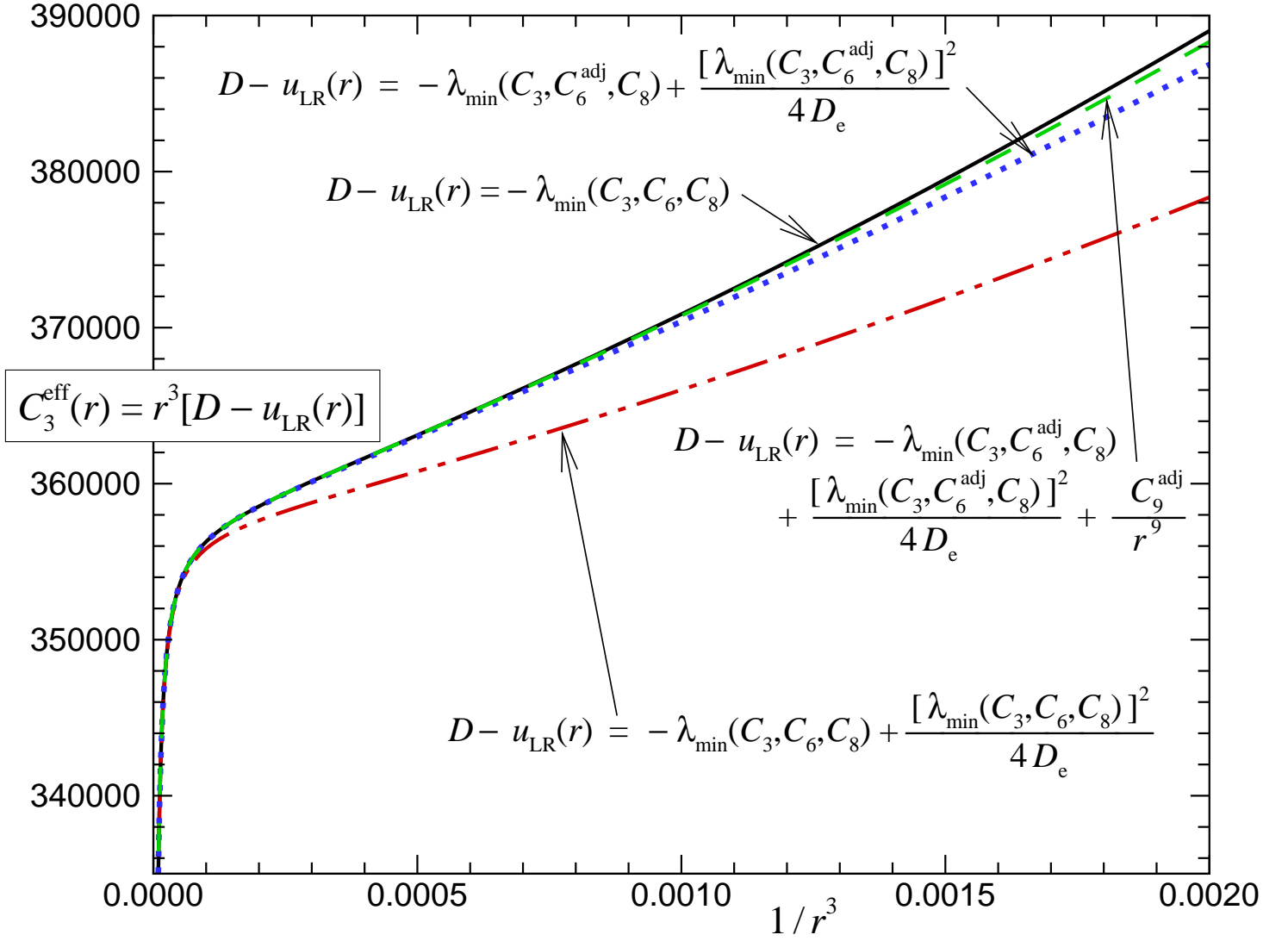


Figure 4: Comparison of four representations of the long-range potential for the $1^3\Sigma_g^+$ state of Li_2 , with energies in cm^{-1} and lengths in \AA .

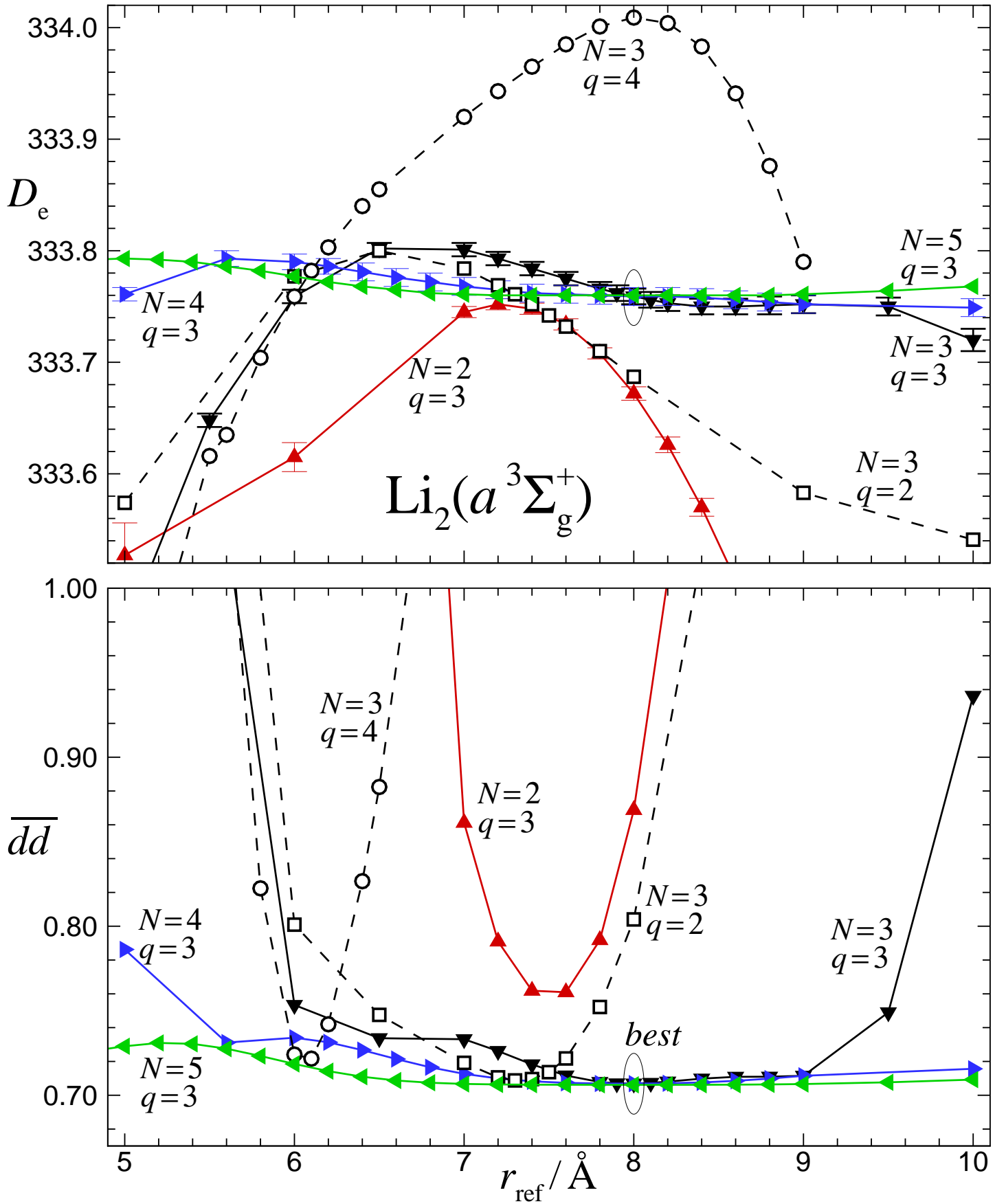


Figure 5: Determination of the optimum model for the $a^3\Sigma_u^+$ state of Li_2 .

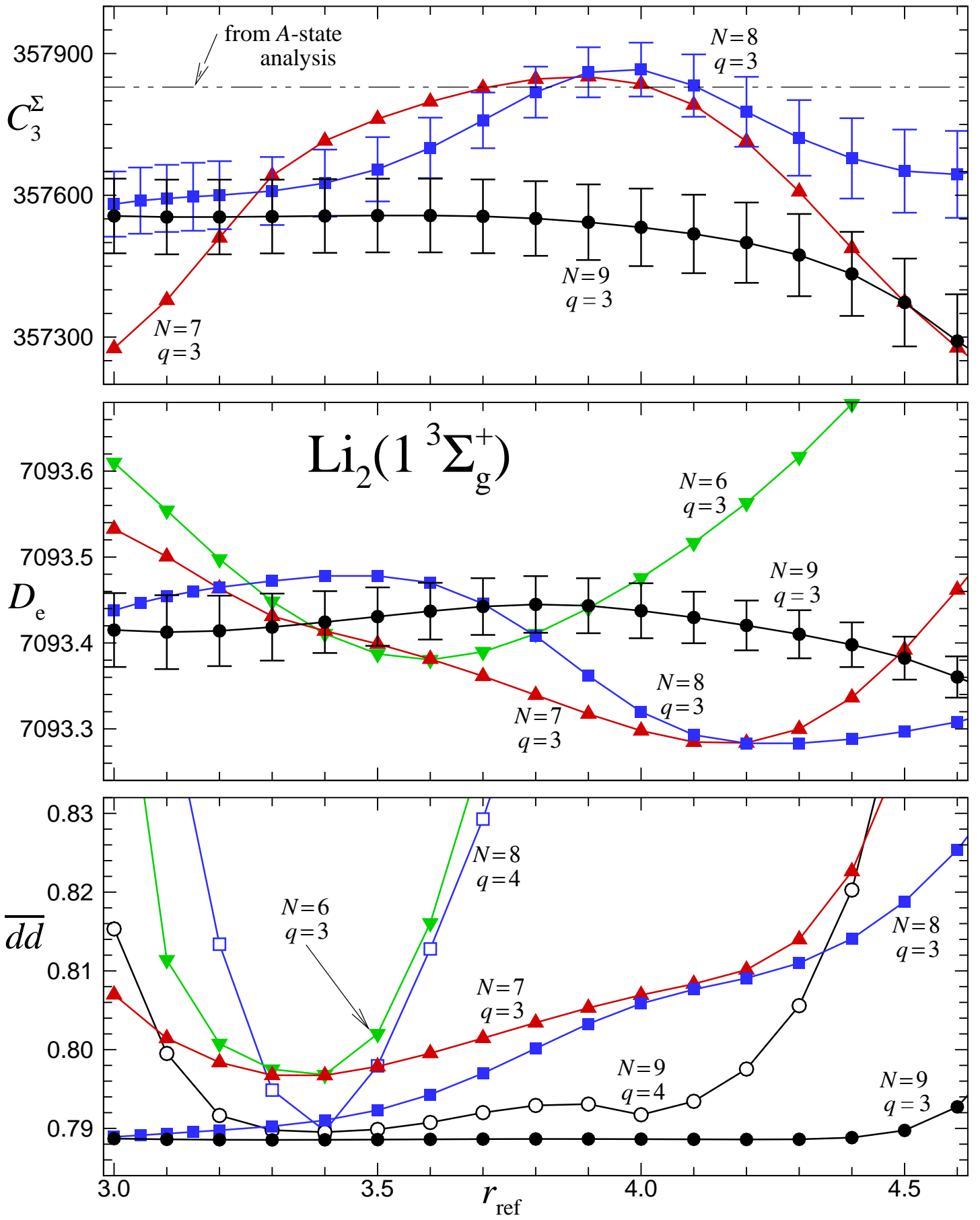


Figure 6: Determination of the optimum model for the $1^3\Sigma_g^+$ state of Li_2 .

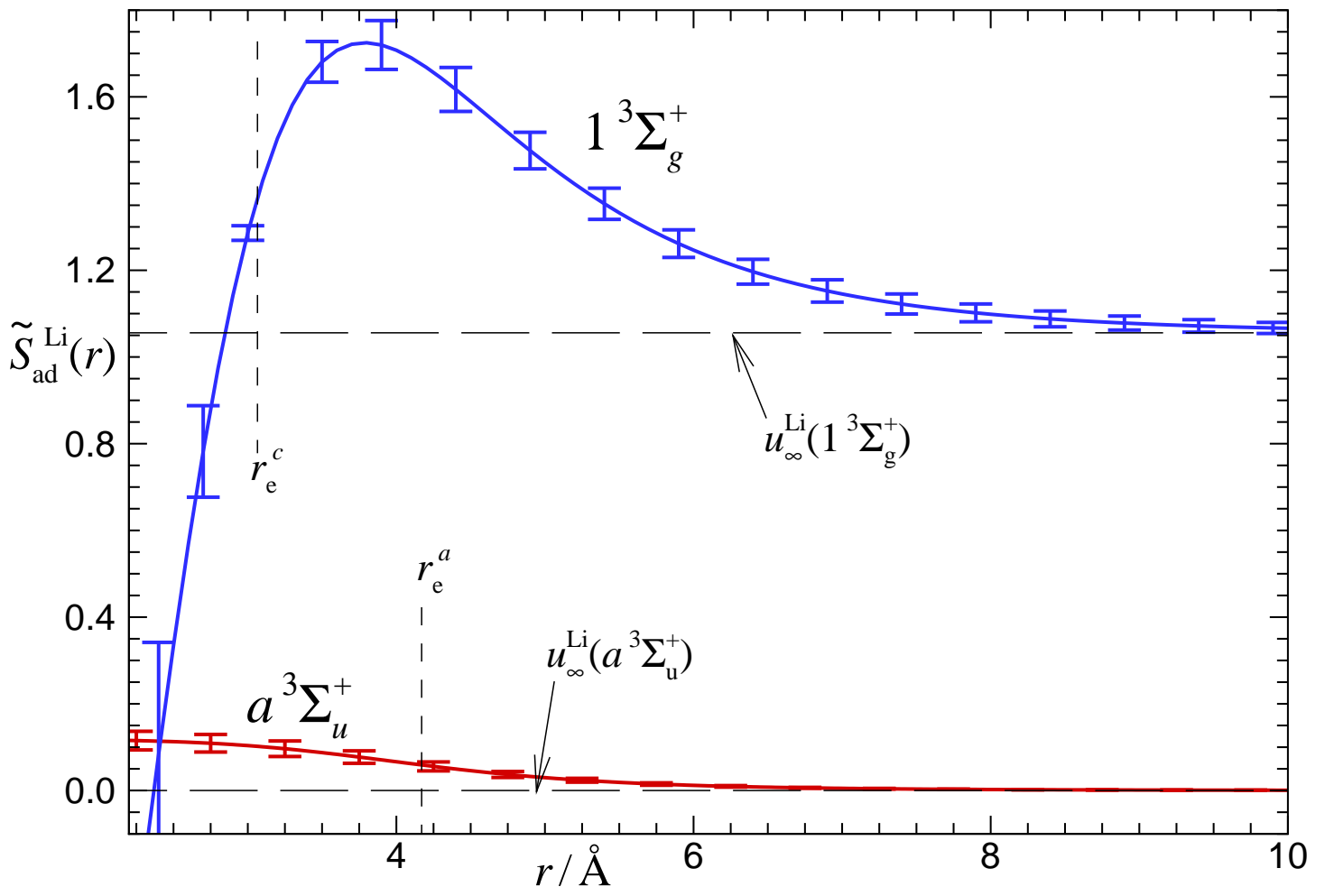


Figure 7: BOB radial strength functions (in cm^{-1}) determined with ${}^7,{}^7\text{Li}_2$ as the reference isotopologue.

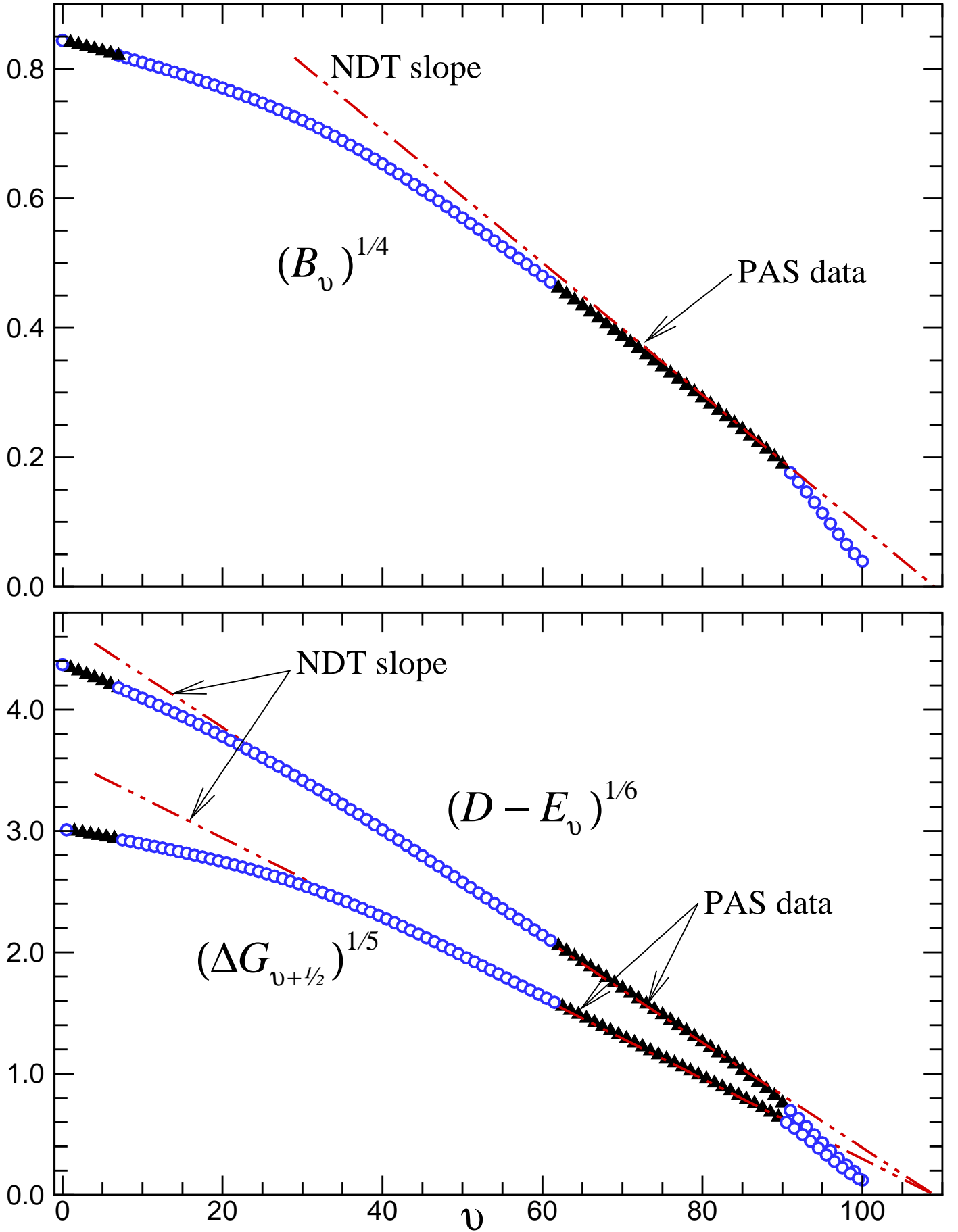


Figure 8: Spectroscopic properties of the $1^3\Sigma_g^+$ state of $^{7,7}\text{Li}_2$.